iScience

CellPress
OPEN ACCESS

Article

Ecological engineering of iron ore tailings into useable soils for sustainable rehabilitation

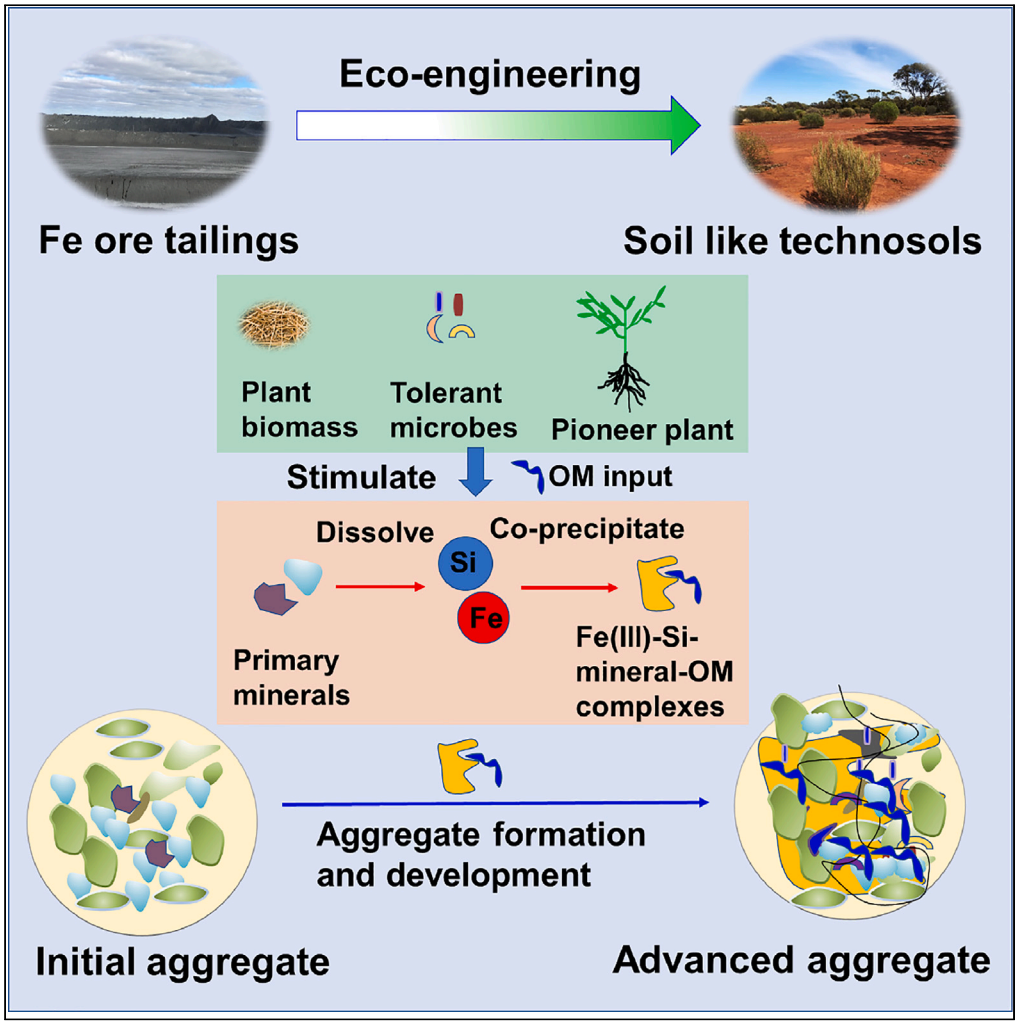

Songlin Wu, Yunjia Liu, Gordon Southam, ..., Narottam Saha, Yong Sik Ok, Longbin Huang

l.huang@uq.edu.au

Highlights

Soil aggregate formation through eco-engineering of inhospitable Fe ore tailings

Microbial and rhizosphere activities drove soil aggregate formation in tailings

Mineral weathering was enhanced and colloidal Fe(III)-Si mineral gel was generated

Conceptual model was proposed for aggregate development with mineral gel as backbone

Wu et al., iScience 26, 107102
July 21, 2023
https://doi.org/10.1016/j.isci.2023.107102

iScience

CellPress
OPEN ACCESS

Article

Ecological engineering of iron ore tailings into useable soils for sustainable rehabilitation

Songlin Wu,[1] Yunjia Liu,[1] Gordon Southam,[2] Tuan A.H. Nguyen,[1] Kurt O. Konhauser,[3] Fang You,[1] Jeremy J. Bougoure,[4] David Paterson,[5] Ting-Shan Chan,[6] Ying-Rui Lu,[6] Shu-Chih Haw,[6] Qing Yi,[1] Zhen Li,[1] Lachlan M. Robertson,[1] Merinda Hall,[1] Narottam Saha,[1] Yong Sik Ok,[1,7] and Longbin Huang[1,8,*]

SUMMARY

Ecological engineering of soil formation in tailings is an emerging technology toward sustainable rehabilitation of iron (Fe) ore tailings landscapes worldwide, which requires the formation of well-organized and stable soil aggregates in finely textured tailings. Here, we demonstrate an approach using microbial and rhizosphere processes to progressively drive aggregate formation and development in Fe ore tailings. The aggregates were initially formed through the agglomeration of mineral particles by organic cements derived from microbial decomposition of exogenous organic matter. The aggregate stability was consolidated by colloidal nanosized Fe(III)-Si minerals formed during Fe-bearing primary mineral weathering driven by rhizosphere biogeochemical processes of pioneer plants. From these findings, we proposed a conceptual model for progressive aggregate structure development in the tailings with Fe(III)-Si rich cements as core nuclei. This renewable resource dependent eco-engineering approach opens a sustainable pathway to achieve resilient tailings rehabilitation without resorting to excavating natural soil resources.

INTRODUCTION

Billions of tons of mine tailings are generated annually from extracting and processing of metal and mineral ores,[1–3] stockpiled in about 4,800 mine tailings storage facilities (TSFs),[4] occupying >240,000 ha of land worldwide.[4] Iron (Fe) ore tailings are one of the most challenging global tailings liability,[5] with over 1.4 billion tons of tailings generated each year.[6] These tailings are not only detrimental to the local environment, but they also have a significant CO_2 footprint associated with rehabilitation and mine closure. Moreover, the traditional soil cover methods consume non-renewable natural soil resources and destroy the local soil ecosystem because of the reliance on excavating and transporting large volumes of soil from natural landscapes.

Although Fe-ore tailings pose little pollution risks of heavy metals (unlike metal mine tailings, such as Pb-Zn tailings), they are not suitable for direct colonization of soil microbes and plants. This is because of their finely textured and highly compacted physical structure, and adverse chemical properties (i.e., alkaline pH, saline conditions, low organic matter and available nutrients).[7] Past efforts to revegetate tailings have largely failed, because the effectiveness of remediation methods were short-lived, without accelerating pedological processes (e.g., mineral weathering and aggregation) for soil structure and hydrogeochemical stability development in the tailings.[8] A sustainable approach is urgently required to carry out ecological rehabilitation of Fe ore tailings storage dams without secondary damages to natural landscapes for soil excavation.

Evidence so far has demonstrated that one way forward is to develop tailings into soil-like substrates (termed herein technosol) with soil structures capable of supporting sustainable vegetation cover.[7,9] This approach adopts ecological engineering (eco-engineering) using abiotic and biotic inputs (i.e., organic matter, pioneer plants, soil microbes, and irrigation) within the context of soil pedogenesis.[9] The critical step in this eco-engineering process is to initiate and accelerate formation of functional soil aggregates in the finely textured tailings, for diverse plant colonization.[10]

[1]Centre for Mined Land Rehabilitation, Sustainable Minerals Institute, The University of Queensland, Brisbane, QLD 4072, Australia

[2]School of Earth & Environmental Sciences, The University of Queensland, Brisbane, QLD 4072, Australia

[3]Department of Earth & Atmospheric Sciences, University of Alberta, Edmonton, AB T6G 2E3, Canada

[4]Centre for Microscopy, Characterisation and Analysis, University of Western Australia, 35 Stirling Hwy, Crawley, Perth, WA 6009, Australia

[5]Australian Synchrotron, Melbourne, VIC 3168, Australia

[6]National Synchrotron Radiation Research Centre, Hsinchu Science Park, Hsinchu 30092, Taiwan

[7]Korea Biochar Research Center, APRU Sustainable Waste Management Program & Division of Environmental Science and Ecological Engineering, Korea University, Seoul 02841, Korea

[8]Lead contact

*Correspondence: l.huang@uq.edu.au

https://doi.org/10.1016/j.isci.2023.107102

Stable and functional aggregates are key physical units underpinning the development of soil structure for regulating water retention, gaseous exchanges, soil organic matter and nutrient dynamics and biology capacity (e.g., root penetration and microbial colonization).[11,12] The formation of soil aggregates involves assemblage of soil clay mineral particles with organic matter in natural soil.[11] Previous studies with natural soil aggregates have emphasized the role of transient organic cements rather than mineral cements in the formation and stability of soil aggregates.[13,14] In fact, ferric iron (Fe(III))-rich amorphous minerals have been considered as potentially important reagents contributing to aggregation in natural soil formed from Fe-rich parent lithologies.[15,16] Microbes and plants play critical roles in stimulating bioweathering of primary minerals, especially ferrous iron (Fe(II))-bearing phyllosilicates and the generation of amorphous Fe(III) rich secondary minerals.[17,18] Iron ore tailings can be treated as engineered parent materials rich in Fe bearing phyllosilicates, such as biotite and amphibole, without risks of heavy metal toxicity.[7] These primary minerals can be weathered to secondary and amorphous Fe(III) rich mineral cements[19,20] because of microbial and rhizosphere activities.[19,21] These amorphous Fe(III) minerals act as core nuclei for cementing together finely textured mineral particles, adsorbing and sequestering organic carbon, and forming water-stable aggregates. As a result, it is critical to resolve how to initiate and accelerate the generation of amorphous Fe(III) mineral cements for aggregating fine mineral particles and sequestering organic matter into Fe ore tailings.

In the present study, we demonstrate stable aggregate development in the Fe ore tailings through an eco-engineering procedure initiated with tolerant microbes and pioneer plants. It was found that the aggregate stability increased with more colloidal Fe(III)-silica (Si) rich amorphous minerals in the tailings. The amorphous Fe(III)-Si cement formation could be stimulated through continuous microbial and rhizosphere driven biogeochemical processes. By comparing the newly formed aggregate structure in tailings with those of native Fe rich soils, we then develop a conceptual model for stable aggregate development resulting from continuous generation and accumulation of Fe(III)-Si rich cement during mineral weathering of the Fe ore tailings. We propose that this process is the critical step toward the development of soil structure for ecological rehabilitation.

RESULTS

Physical and chemical changes in tailings subject to eco-engineering inputs

In a glasshouse experiment, rapid pH neutralization was achieved and geochemical properties were improved within one month after amending alkaline Fe-ore tailings with 2% (w/w) Lucerne hay (shoot biomass of Alfalfa, *Medicago sativa*) and native soil microbes (Figure 1, Table S1A). The resultant tailings were sufficiently improved to have developed physical and chemical conditions to accommodate successful colonization by pioneer plant species for 3.5 months (Figure 1, Table S1A), including *Atriplex amnicola*, *Maireana brevifolia*, and *Sorghum* spp. Hybrid cv. Silk. By this stage the eco-engineered tailings are considered as an "early technosol" supporting the proliferation of pioneer plants (Figure 1). The colonizing pioneer plants further advanced the development of "early technosol" toward "advanced technosol" through rhizosphere driven biogeochemical processes, leading to further improved physical and chemical properties in tailings (Figure 1, Table S1). The "advanced technosol" is expected to be structurally and functionally capable of supporting the colonization of diverse native keystone plant species and rhizosphere microbes such as mycorrhizal symbiosis. These accumulative impacts of microbial and rhizosphere processes in the technosol significantly ($p < 0.05$) shifted the development of key physical and chemical properties away from those in the initial tailings (Figures 2A and 2B; Table S1) and toward the onset of early and advanced technosol (ANOSIM test, $p < 0.05$; Figure 2B). Typically, the pH decreased from extreme alkaline (>9.5) in initial tailings to circumneutral (8.5–8.9) in "early technosol" and "advanced technosol" ($p < 0.05$). Total organic carbon (TOC) concentration increased from <0.5 g kg^{-1} to 2–4 g kg^{-1} in technosols ($p < 0.05$, Table S1). Plant colonization decreased electrical conductivity (EC) value significantly in "advanced technosol" ($p < 0.05$, Tables S1B and S1C). However, at this stage the resultant "advanced technosol" have not yet reached the same property state of native Fe-rich soil at the Fe ore mine site according to principal component analysis (PCA) of physical and chemical variation (ANOSIM test, $p < 0.05$; Figure 2B).

According to PCA analysis, macroaggregate percentage and MWD value were key contributors to PC1 (contributing 54.3% of the variation). Similarly, microaggregate percentage was the dominant contributor to PC2 (contributing 19.7% of the whole variation) (Figure 2A). These values indicate that aggregate stability (physical property) was the dominant factor differentiating properties of tailings, technosols,

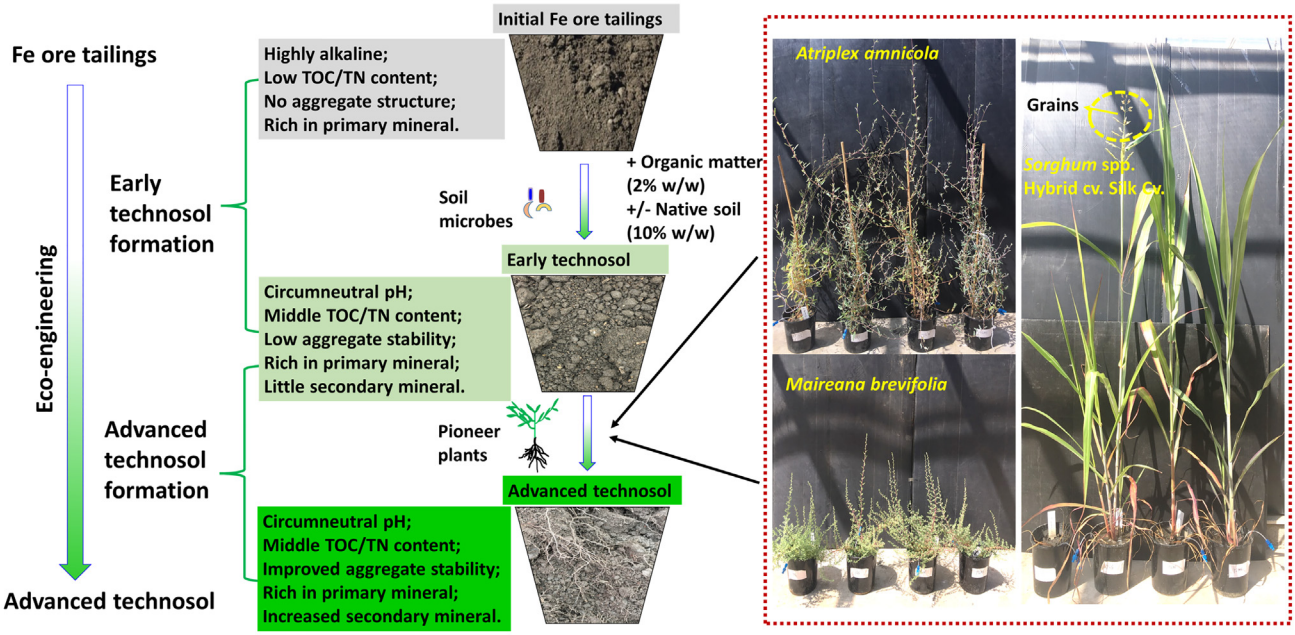

Figure 1. A schematic diagram illustrating the eco-engineering Fe ore tailings into soil-like substrates

Process of "early technosol" formation – characteristic of organic matter and microbial inoculation inputs for pH neutralization, geochemical improvement, and alleviation of physical compaction (early aggregate formation). The "early technosol" can support colonization of pioneer tolerant plants. Process of "advanced technosol" formation – characteristic of the development of well buffered geochemical properties and improved physical structures (advanced aggregate formation). The "advanced technosol" is expected to be structurally and functionally capable of supporting the colonization of diverse native keystone plant species and associated microbes. The photos on the right show growth of *Atriplex amnicola*, *Maireana brevifolia*, and *Sorghum* spp. Hybrid cv. Silk. in tailings for 3.5 months after transplantation.

and native soil. Furthermore, the percentage of macro- and micro-aggregates, as well as the value of mean weight diameter (MWD, a common indicator of soil aggregate stability[11] and soil physical functionality[22]) increased progressively during the eco-engineering processes toward technosol formation ($p < 0.05$, Figures 2C–2E).

Microstructure and cementation of aggregates formed in "early technosol"

There was a heterogeneous distribution pattern of small-sized and irregular Fe-bearing minerals adhered onto quartz particles within macroaggregates (Figures 3A–3C). The Fe concentrations varied from 0 to 50% w/w (Figures 3B and 3C) across selected aggregate transections as revealed by synchrotron-based X-ray fluorescence microscopy (XFM) analysis. The Fe-bearing minerals were closely associated with biotite, amphibole and FeOx (representing Fe oxides and/or hydroxides), according to the mineral liberation analyzer (MLA) and BSE-EDS analyses (Figures 3D–3H), which were distributed randomly amongst the quartz grains. The dominant presence of biotite (a K rich mica) was further supported by the strong Fe-K association (i.e., areas with Fe: K ratio of ~9.98) in the tri Fe-K-Ca mapping (Figure S1) and correlation mapping (Figure S2). Little mineral cement was detected in adjoining spaces surrounding primary mineral particles in the tailings (Figures 3D and 3F). As characterized by synchrotron-based C 1s NEXAFS analysis (Figure 3I) and high resolution C 1s XPS (Figure S3), the organic carbon (OC) in the aggregates formed in the "early technosol" were mainly composed of aromatic, carboxyl, phenolic, alkyl and O-alkyl rich compounds. The NanoSIMS analysis revealed that those OC in the aggregates was heterogeneously distributed at micron scale and mainly associated with Fe rich minerals (Figures 3J–3L).

Microstructure and cementation of aggregates formed in "advanced technosol"

During the "advanced technosol" formation, the percentage of microaggregates and MWD value increased significantly in response to colonization of various plant species ($p < 0.05$, Figure 2D), except for *Sorghum* spp. plants that could not survive in "early technosol" without 10% (w/w) native soil amendment (Figure S4). The aggregates in the "advanced technosol" contained mostly quartz and biotite,

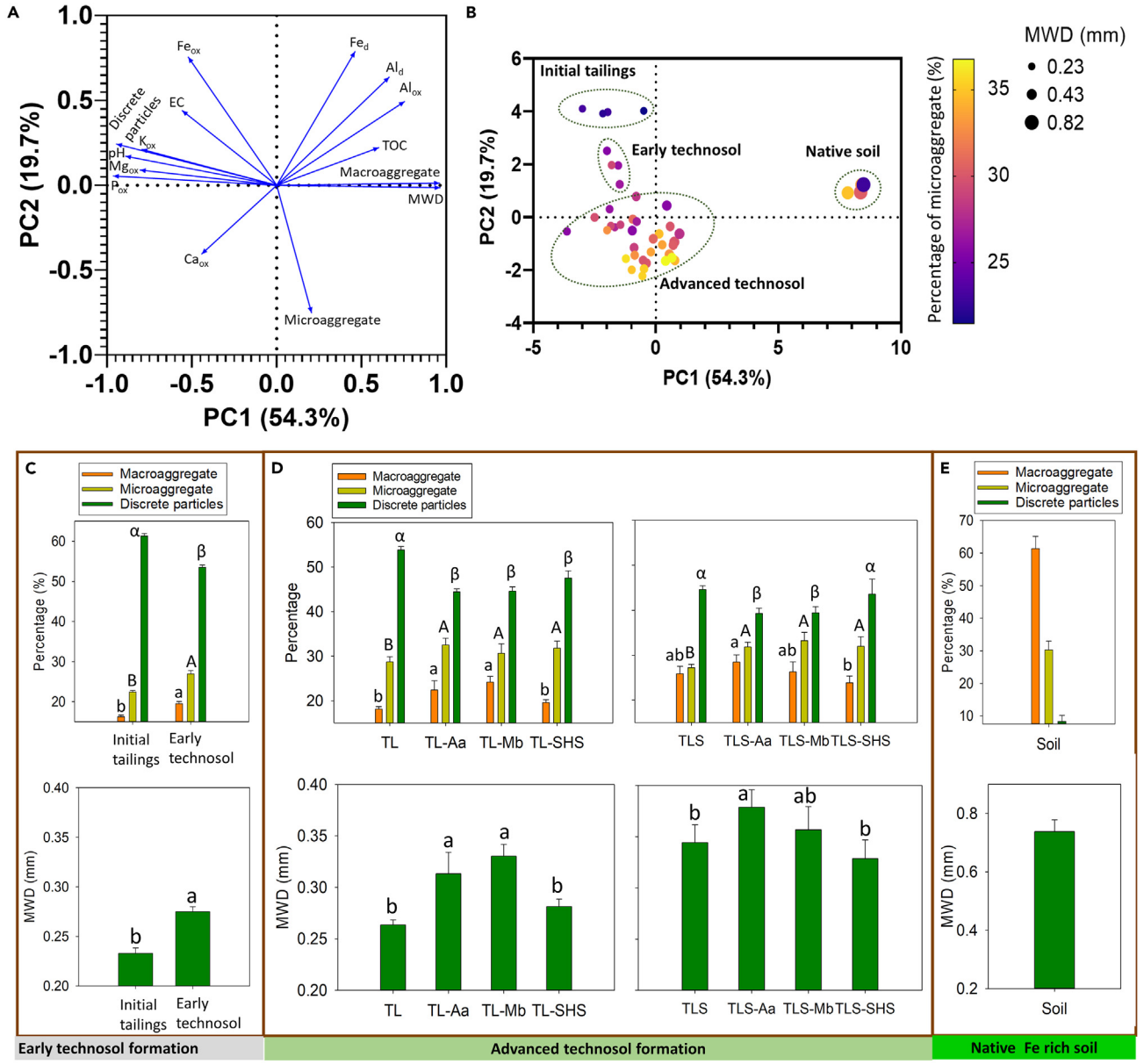

Figure 2. Overall variations of physical and chemical properties, as well as water stable aggregate distribution in the tailings, technosols and the native soil

(A and B) Principal component analysis (PCA) of physical and chemical characteristics (pH, EC, TOC, Fe_{ox}, Al_{ox}, Fe_d, Al_d, P_{ox}, K_{ox}, Mg_{ox} and Ca_{ox}, as well as aggregate fractions and stability, all data were standardized) in initial tailings, "early technosol", "advanced technosol" and native soil. ANOSIM test indicates the significant difference between tailings/technosols and native soils ($R = 0.999$, $p = 0.001$), initial tailings and early technosol ($R = 1$; $p = 0.02$), initial tailings and advanced technosol ($R = 0.999$, $p = 0.001$), early technosol and advanced technosol ($R = 0.807$, $p = 0.001$).

(C–E) The distribution and mean weight diameter (MWD) of water stable aggregates in (c) early technosol, (d) advanced technosol, and (e) native Fe rich soil surrounding the tailing site. The water stable aggregate classification: macroaggregates (250–2000 μm), microaggregates (53–250 μm), discrete particles (<53 μm). Data are represented as mean ± SEM. Different letters above the columns show significant difference between different treatments based on Tukey test at $p < 0.05$.

Note: "TL", Tailings + Lucerne hay (2% w/w); "TLS", Tailings + Lucerne hay (2% w/w) + Native soil (10% w/w); "Aa", *Atriplex amnicola*; "Mb", *Maireana brevifolia*; "SHS", Silk sorghum grass (*Sorghum* spp. Hybrid cv. Silk).

amphibole and FeOx, but more irregular Fe-Si rich minerals were found in the pore sites surrounding those primary mineral particles within microaggregates from pioneer plant colonized technosols (Figure 4).

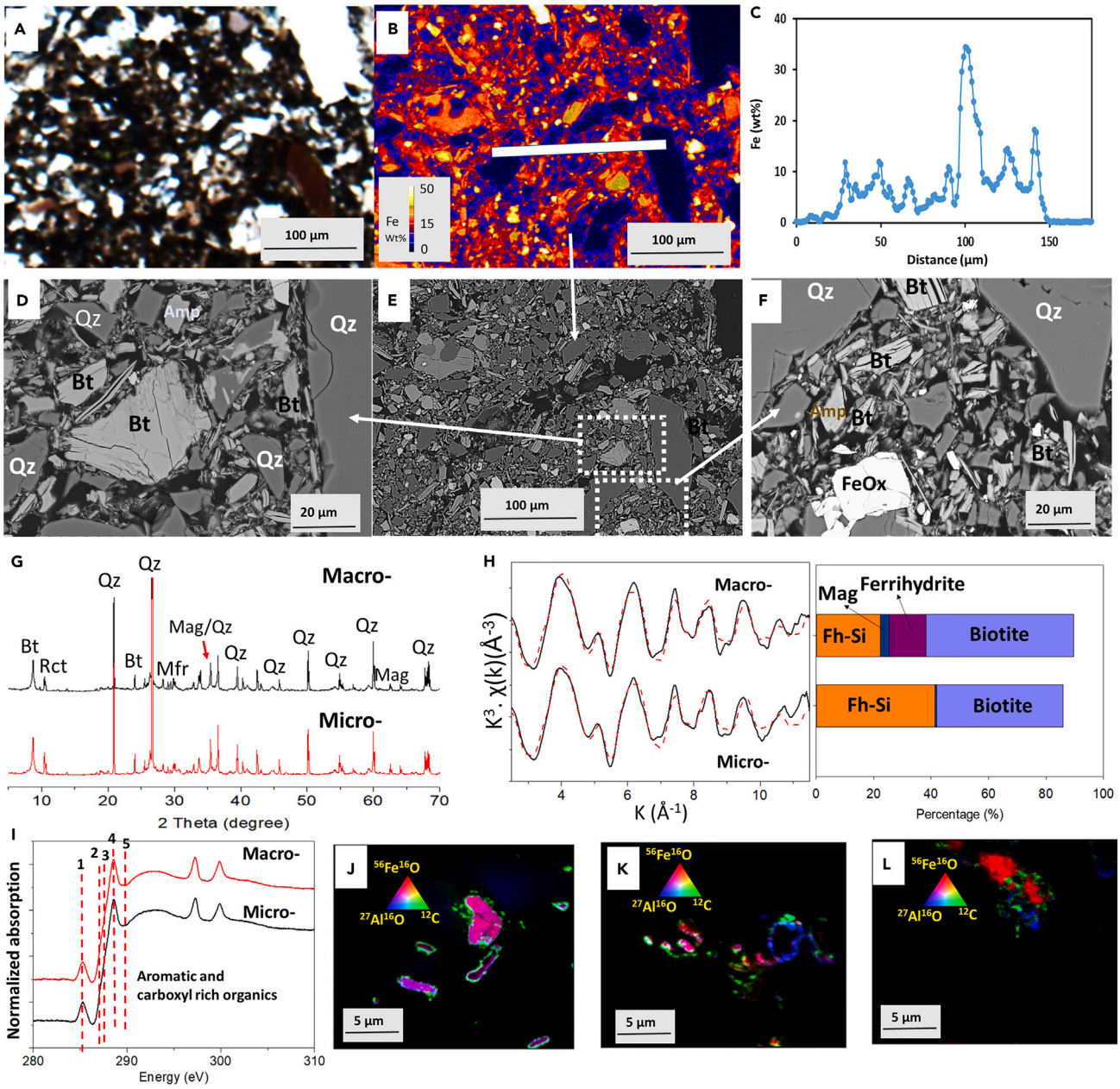

Figure 3. The microstructure of aggregates from the "early technosol" as revealed by synchrotron based X-ray fluorescence microscopy (XFM), mineral liberation analysis (MLA), and backscattered-scanning electron microscope-energy dispersive X-ray spectroscopy (BSE-SEM-EDS) analysis

(A) A thin section of tailing macroaggregates under light microscopy.

(B) Fe mapping of the tailing macroaggregate thin sections as revealed by XFM analysis.

(C) Fe concentrations across the selected area of the thin sections of aggregates in "b" (the distance in X axis is from the left to the right).

(D–F) BSE-SEM images showing the microstructure of the aggregates and their mineral distribution.

(G) XRD spectra of macroaggregates (250–2000 μm) and microaggregates (53–250 μm) in early technosol eco-engineered from tailings. Note: Qz = Quartz; Mag = magnetite; Bt = Biotite ($K(Mg,Fe)_3(AlSi_3O_{10})(F,OH)_2$); Rct = Richterite ($((Na,K)_2(Mg,Mn,Ca)_6Si_8O_{22}(OH)_2$), an amphibole; Mfr = magnesioferrite ($(Mg(Fe^{3+})_2O_4$), FeOx = Fe oxides, and/or hydroxides.

(H) *k* space Fe K-edge EXAFS spectra (weight 3) (line) and linear combination fitting (LCF, dashed) of early technosol aggregates. The right column shows the results of the fitting Fe K-edge EXAFS spectra. The fitting parameters: For Macro-aggregate: R factor = 0.069, Chi-square = 41.6, Reduced chi-square = 0.23; For Micro-aggregate: R factor = 0.092; Chi-square = 50.6; Reduced chi-square = 0.28.

Figure 3. *Continued*

(I) Synchrotron based C 1s NEXAFS spectra of aggregates from early technosol. Note: 1, 285.2 eV, aromatic C; 2, 286.5 eV, phenolic, pyrimidine or imidazole C; 3, 287.4 eV, alkyl C; 4, 288.3 eV, carboxyl C; 5, 289.3 eV, O-alkyl C.

(J–L) Two-dimensional NanoSIMS images for the dispersed aggregates from early technosol. The red is $^{56}Fe^{16}O$, the green is ^{12}C, and the blue is $^{27}Al^{16}O$. The range of counts for these images are: $^{56}Fe^{16}O$, 0–300; ^{12}C, 0–100; $^{27}Al^{16}O$, 0–120.

The increasing accumulation of mineral cements in aggregates was further delineated through detailed examination of the mineralogy and OC forms in different fractions of microaggregates (i.e., colloidal and non-colloidal fraction) in comparison with that in bulk tailings (Figures 5 and 6). According to the linear combination fitting (LCF) of Fe K edge XAFS spectra, minimal changes in Fe phases were detected in the bulk tailings, which was mainly composed of biotite and magnetite-like minerals, regardless of tailings treatments (Figures 5A and S5). The proportion of biotite-like minerals decreased in colloidal and non-colloidal fraction of microaggregates, compared to that in the bulk tailings (Figure 5A). This was further confirmed by XRD analysis that revealed the reduction of crystalline primary minerals (i.e., biotite and amphibole minerals) and the emergence of mixed layered minerals (such as illite and smectic groups) in the colloidal and non-colloidal fractions of the microaggregates (Figures 5B and S6). By contrast, Fe(III)-Si-short range ordered (SRO) like minerals were found to be dominant in the colloidal fraction (Figure 5A); they appeared to be around 10 nm in size and were identified as Fe-Si rich poorly crystalline minerals (Figures 5C and S7).

Plant colonization in the tailings consistently increased the percentage of the colloidal fraction in the microaggregates (Figure 5D) and the proportion of Fe(III)-Si-SRO like minerals within the colloidal fraction (Figure 5A). Ferrous iron (Fe(II)) oxidation into Fe(III) (Figure S8), and coupled co-precipitation with silica, formed a highly amorphous structure with few double corner interactions around the Fe core (Figure S9). This presented a high capability for further interactions with organics and other minerals.

These colloidal Fe(III)-Si-SRO minerals were readily associated with organic carbon as evidenced by elevated OC contents in colloidal fraction, compared to those in the non-colloidal fraction of microaggregates and bulk tailings (Tables S1 and S2). The functional groups of the organics within microaggregates were mainly composed of carboxyl, alkyl, O-alkyl, carbonyl, and aromatic groups in both colloidal and other fractions (Figures 6 and S10). Comparatively, plant colonization increased the percentage of aromatic, carboxylic, and carbonyl groups, but decreased the percentage of O-alkyl groups (from polysaccharides) in the colloidal fraction, as revealed by synchrotron C 1s NEXAFS analysis (Figure 6). This was confirmed by ATR-FTIR analysis, which revealed that plant colonization enhanced peaks at around 1633 cm^{-1} and 1423-1436 cm^{-1}[23] (Figure S11), indicating the possible association of aromatic and/or carboxyl groups with minerals (such as Fe(III)-Si rich SRO minerals) in the rhizosphere colloidal fraction.

Geochemical changes during rhizosphere driven "advanced technosol" formation

The plant colonization altered geochemical characteristics of the tailings porewater. Generally, the porewater pH was circumneutral (7.2–8.2) but it was generally increased by plant colonization with time (Figure S12, $p < 0.05$). By contrast, the electrical conductivity (EC) value was decreased by plant colonization with time ($p < 0.05$, Figure S12). Porewater TOC and TN concentrations increased with time, but they were generally reduced by plant colonization (Figure S12). Oxalic, formic, acetic, citric, lactic and tartaric acids were observed in tailings porewater (Figure S13). Plant colonization generally decreased oxalic acid concentration but increased acetic acid concentration in porewater (Figure S13, $p < 0.05$). The concentrations of K and Mg in porewater were 10-1,000 times higher than that of Fe, Al and Si (Figure S14). Plant colonization generally increased porewater Fe, Al, K and Mg concentrations during the first month, but decreased (or had no effects on) those elemental concentration after 2 months' cultivation (Figure S14, $p < 0.05$). Consistently, plant shoots and roots took up high quantities of K, Mg, Fe and Al from the tailing technosols (Tables S3 and S4).

Rhizosphere microbial community development in "advanced technosol"

As plant colonization drove the development of the "early technosol" toward the "advanced technosol", the prokaryotic microbial community diversity and composition shifted (Figure 7). According to Illumina sequencing, there were above 15,000 reads for all tailing samples, which were classified into 150–800 OTUs based on 97% sequence (Figure S15). The Rarefaction curves showed that the depth of the sequencing for tailings and technosol samples was adequate for characterizing prokaryotic microbial

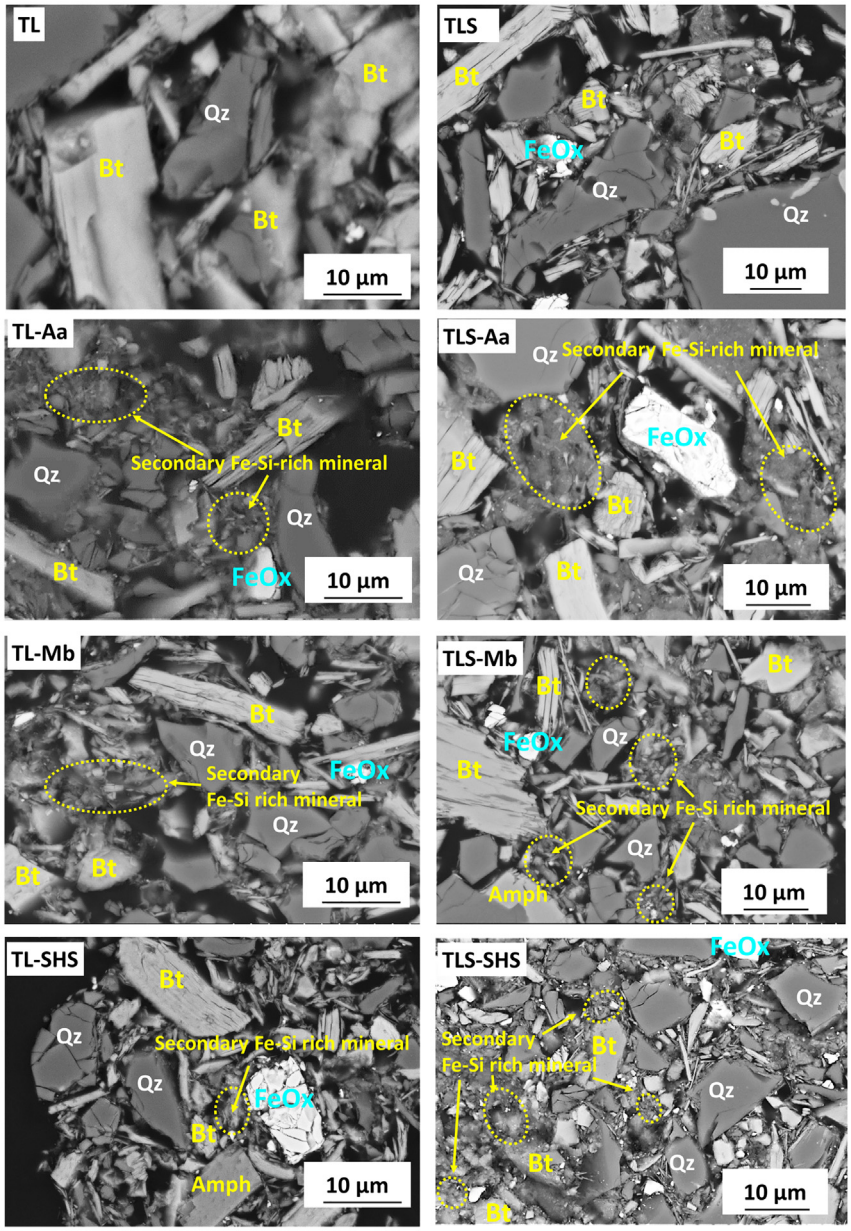

Figure 4. Backscattered-scanning electron microscope (BSE-SEM) showing the structure of the microaggregates from "advanced technosol" with various plant colonization treatments

Note: the meanings of "TL", "TLS", "Aa", "Mb" and "SHS" are shown in the caption of Figure 2. For the minerals in BSE figures (verified by mineral liberation analysis, energy-dispersive spectroscopy, and X-ray diffraction analysis), "Bt" represents biotite, "FeOx" represents Fe oxides, and/or hydroxides; "Qz" represents quartz; "Amph" represents amphibole. Black areas are organic matter that has infilled pore spaces.

communities (Figure S15). The OTU richness increased dramatically from round 200 in "early technosol" to above 400 in "advanced technosol" ($p < 0.05$, Figure S16). The Shannon index of microbial community increased from ca. 3.6 in "early technosol" to >5.5 in "advanced technosol" ($p < 0.05$, Figure S16). Neither soil amendment nor plant colonization influenced microbial diversity (Figure S16).

Compared with "early technosol", the "advanced technosol" contained more Acidobacteria, Bacteroidetes, Chloroflexi, Cyanobacteria, Planctomycetes and Verrucomicrobia, but less Proteobacteria and Firmicutes (Figure 7A). Furthermore, plant colonization resulted in different microbial community patterns

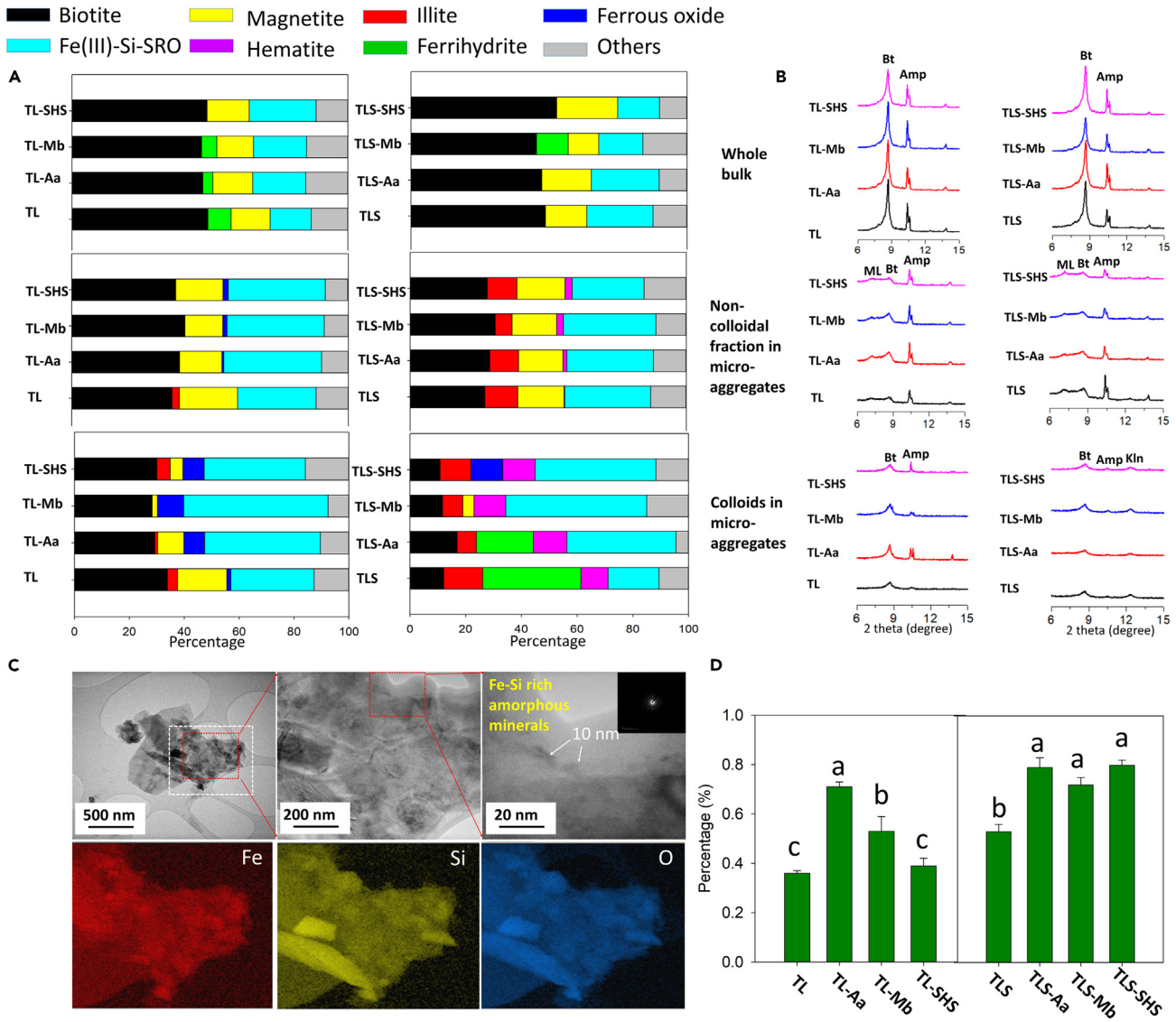

Figure 5. Mineral phases and morphology in different fractions of "advanced technosol" subject to different plant colonization treatments

(A) Fe phases in bulk tailings, colloids and non-colloidal fraction (the mineral deposits left after colloid extraction) in microaggregates, as revealed by linear combination fitting (LCF) of *k* space Fe K-edge EXAFS spectra (k weight 3) (EXAFS spectra and LCF fitting parameters are in Figure S5).

(B) XRD spectra (2 theta 6-15°) of whole bulk tailings, colloids and non-colloidal fractions in microaggregates from different treatments (Note: Bt = Biotite; ML = Mixed layered mineral such as illite and smectite group; Amp = Amphibole such as richterite; Kln = Kaolinite).

(C) Transmission electron microscopy coupled with selected area electron diffraction and energy-dispersive X-ray spectroscopy (TEM-SAED-EDS) results showing nanophases in colloids of the "advanced technosol" with *Maireana brevifolia* colonization. The electronic diffraction is superimposed on 20 nm scale bright-field TEM images, indicating the presence of amorphous nanosized Fe(III)-Si mineral structure in colloids of microaggregates.

(D) Percentage of colloids in microaggregates from "advanced technosol" with different plant colonization treatments. Data are represented as mean ± SEM. Note: the meanings of "TL", "TLS", "Aa", "Mb" and "SHS" are shown in the caption of Figure 2. Different letters show significant difference between different treatments based on Tukey test ($p < 0.05$).

according to PCA analysis (ANOSIM test, $p < 0.05$, Figure 7B). Plant colonization increased percentage of microbes involved in mineral weathering, such as Verrucomicrobiaceae (belong to phylum Verrucomicrobia),[24] endolithic Ellin6075 (belong to phlum Acidobacteria),[25] Xanthomonadaceae (belong to phylum Proteobacteria, reported to be OM degrader[26]) and Comamonadaceae (order-Burkholderiales)[27] at family level (Figure S17). At genus level, some well-known mineral weathering bacteria such as *Bacillus* spp., *Helothiobacillus* spp., *Solibacillus* spp., *Streptomyces* spp., *Geobacter* spp., *Thiobacillus* spp., and *Mycobacterium* spp.[18] were induced by pioneer plant (such as *M. brevifolia*) colonization (Table S5).

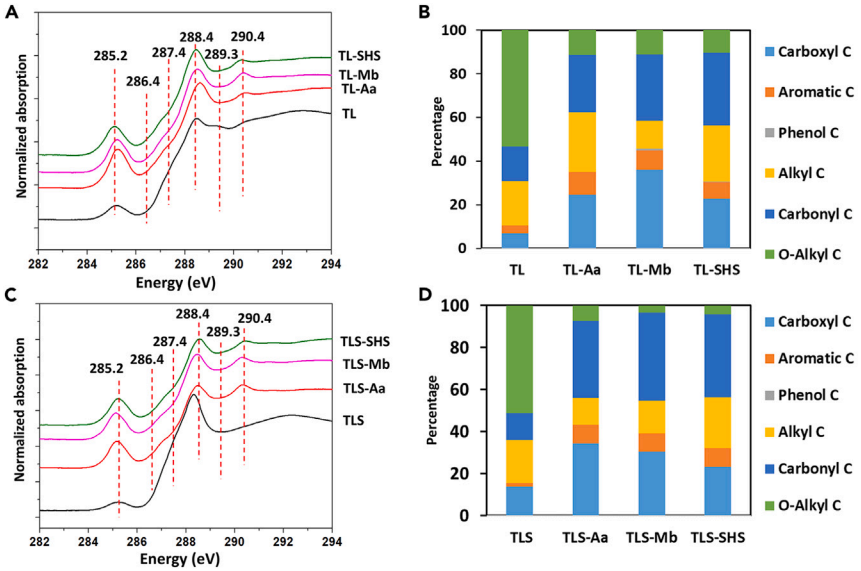

Figure 6. Organic carbon forms in colloidal fractions within microaggregates from "advanced technosol" subject to various plant colonization treatments

(A and C) Synchrotron based C 1s NEXAFS spectra of colloidal fraction. Note: 285.2 eV, aromatic C; 286.4 eV, phenol C; 287.4 eV, alkyl C; 288.4 eV, carboxyl C; 289.3 eV, O-alkyl C; 290.4 eV, carbonyl C.

(B and D) The column plots showed the proportion of different organic C forms as analyzed by peak fitting.

Note: the meanings of "TL", "TLS", "Aa", "Mb" and "SHS" are shown in the caption of Figure 2.

Microstructure and cementation of aggregates in Fe rich native soil

Mineral particles in native soil aggregates were consistently surrounded and cemented together by Fe-Si rich minerals within soil aggregates. The Fe concentrations across the section of soil aggregates accounted up to 10% w/w, with a high degree of spatial heterogeneity (Figures 8A–8C). BSE-SEM-EDS confirmed that the individual quartz grains were cemented by Fe(III)-Si rich cements (Figures 8E–8I). Further MLA, XRD and Fe K edge XAFS analyses indicated that the Fe(III)-Si rich cements were composed of a mixture of Fe(III)-rich amorphous minerals (ferrihydrite-silica complexes) and Fe(III)-bearing clay minerals (i.e., Fe(III)-kaolinite and hematite) (Figures 8D–8K). This structural arrangement was a common feature observed in most of the soil aggregates examined (Figs, S18 and S19), suggesting its ubiquity in the Fe-rich soil aggregates. In addition, some large quartz grains were surface-coated by Fe(III)-Si rich cements (Figure S20), thus promoting chemical reactions with neighboring particles and forming stable and resilient aggregates under natural conditions. According to the three-color mapping of Fe-K-Ca across aggregate sections, the Fe(III)-Si cements were not associated with K or Ca (Figure S21). EDS analysis of the Fe(III)-Si rich cements indicated that the Si: Al ratio was around 1.15 (0.15), and the Si: (Al+Fe) ratio around 0.83 (0.18) (based on the EDS of 20 spots in the Fe(III)-Si rich cements).

As indicated by C 1s NEXAFS analysis (Figure 8L) and C 1s XPS analysis (Figure S22), aromatic, phenolic, carboxyl, aliphatic, O-alkyl and carbonyl groups were found in the soil aggregates. Organic C was primarily located at the surfaces of Fe-rich mineral grains (e.g., Fe oxyhydroxides, Fe bearing kaolinite) in the soil aggregates according to NanoSIMS analysis (Figures 8M and 8N). The XRD and Fe K edge XAFS analysis of soil colloidal fraction and whole microaggregates revealed that those Fe(III)-Si rich minerals were mainly present in the colloidal fraction and composed of mainly Fe-Si-SRO, hematite and Fe(III)-kaolinite (Figure S23). These colloidal particles were around 100 nm in diameter according to FE-SEM analysis (Figure S23).

DISCUSSION

Biological weathering and transformation of minerals are essential processes in natural soil formation.[28] Here, we demonstrated the key drivers including tolerant microbes and pioneer plants in driving eco-engineered soil formation in Fe ore tailings through early and advanced technosol development. By adding a renewable resource, such as plant biomass, into the tailings, heterotrophic microbes can be stimulated to

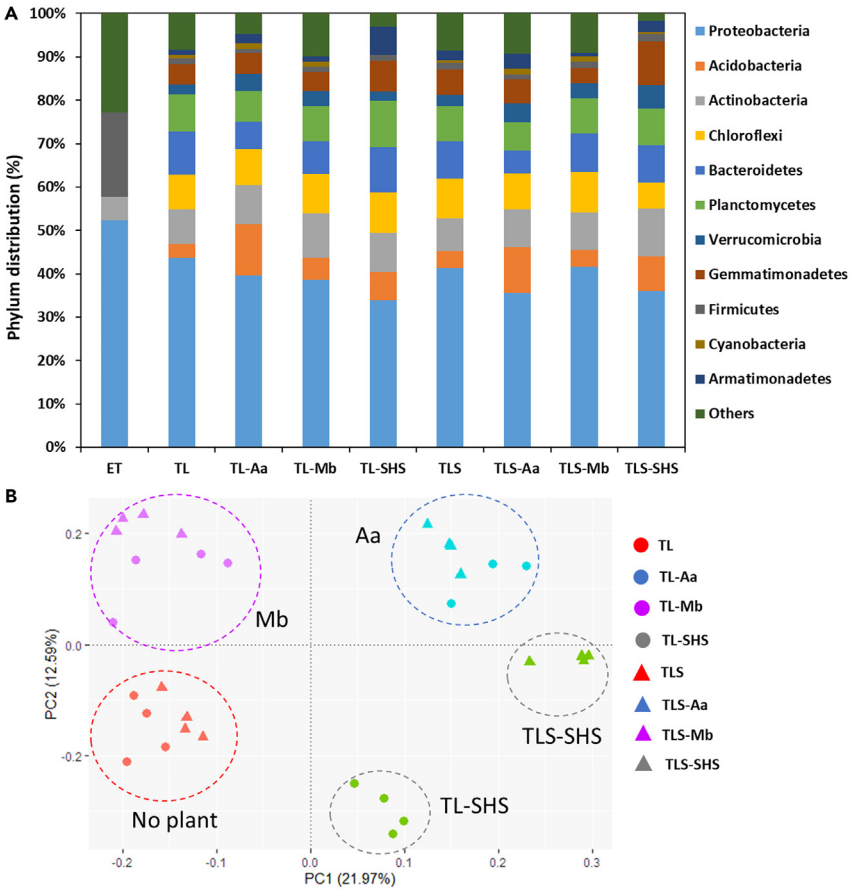

Figure 7. Variations of prokaryotic microbial community in early technosol and advanced technosol subject to different plant colonization treatments

(A) Prokaryotic microbial community composition at the phylum level, and (B) multivariate principal component analysis (PCA) of prokaryotic microbial community (Illumina data) at the OTU level in tailings of different treatments.

Note: "ET", early technosol, the meanings of "TL", "TLS", "Aa", "Mb" and "SHS" are shown in the caption of Figure 2.

decompose organic matter, leading to organic acid generation that not only neutralizes alkaline pH conditions in the tailings, but also facilitates the initial formation of aggregates.[21,29] The functions of tolerance microbial decomposition of exogenous OM stimulated the early pedogenesis, toward forming "early technosol" that is capable of survival of pioneer plants. The colonizing pioneer plants further advanced the development of "early technosol" toward "advanced technosol" (Figure 1) through rhizosphere biogeochemical processes,[19,29–31] leading to improved physical and chemical conditions (Figure 2, Table S1) for various key stone native plant species colonization. Consistent with expected barriers of the compacted tailings, the aggregate stability was the dominant factor differentiating tailings, technosols, and native soil (Figure 2), highlighting the importance of the aggregate development in eco-engineered tailings-soil formation.

Microbial generation of organic cements to initial aggregate formation

Microstructural and microspectroscopic analysis of the tailings undergoing "early technosol" formation revealed that organic cementing agents played a key role in initiating organo-mineral interactions and aggregation of tailings particles, as the extensive mineral weathering of Fe-bearing minerals had not yet occurred to generate secondary mineral cements (Figure 3). In the tailings admixed with OM and the soil inoculum, various chemoheterotrophic microbes, that belong to the phyla of Proteobacteria and Firmicutes, developed and attributed as key OM decomposers in the tailings[32,33] (Figure 7). These tolerant microbes drove the decomposition of added OM even under the extremely alkaline pH conditions in the tailings, producing various organic acids[34] (rich in aromatic, carboxyl, phenolic groups, Figure 3l).

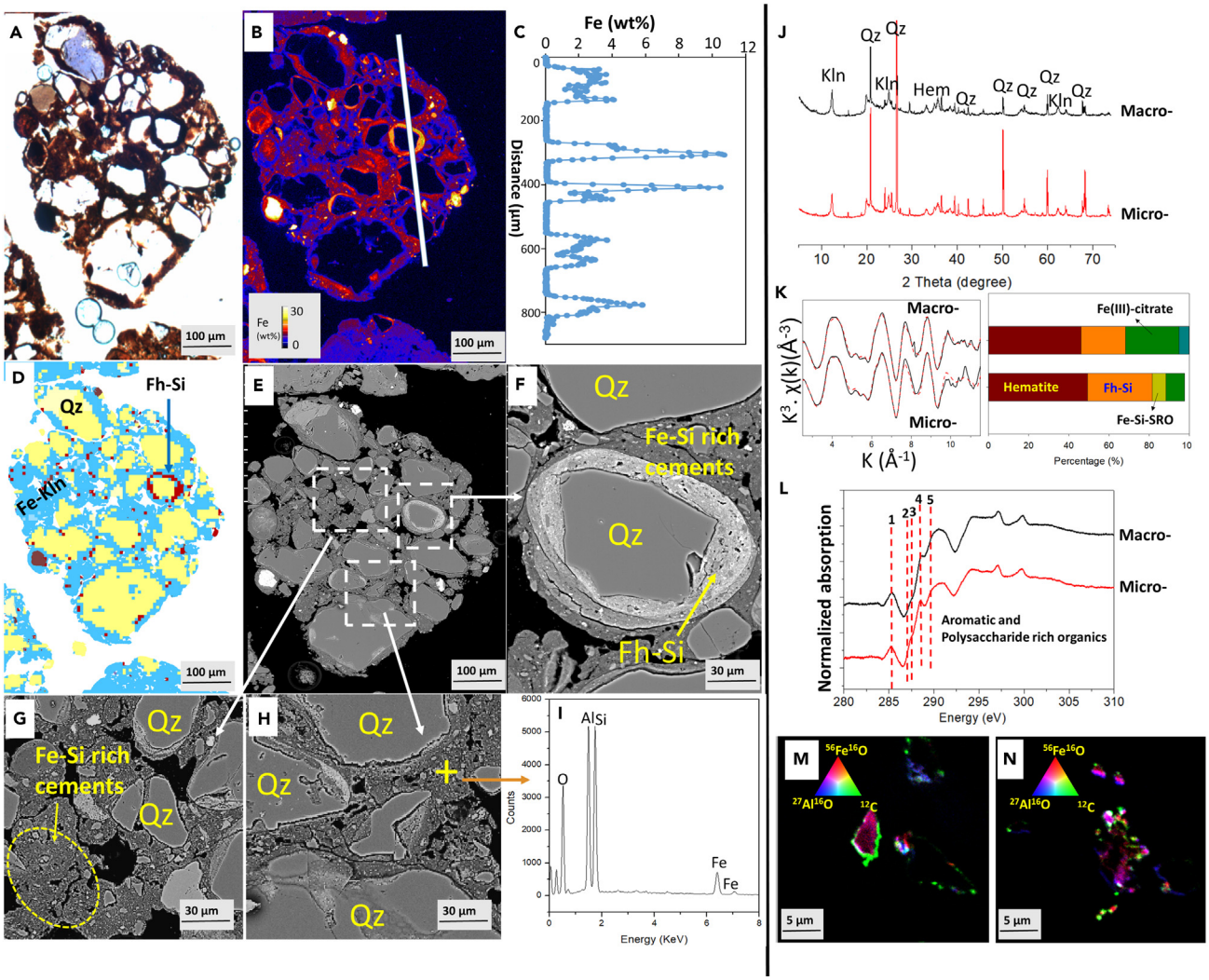

Figure 8. The microstructure of aggregates in natural Fe rich soils surrounding Fe-ore mine site, as revealed by synchrotron based X-ray fluorescence microscopy (XFM), mineral liberation analysis (MLA), and backscattered-scanning electron microscope-energy dispersive X-ray spectroscopy (BSE-SEM-EDS) analysis

(A) Thin sections of aggregates under the light microscope.

(B) Fe mapping as revealed by XFM analysis.

(C) Fe concentrations across the selected area (white line) in "b", the distance in X axis representing top of thin section to bottom.

(D) MLA mapping of different minerals in soil aggregates (yellow is quartz (Qz), blue is Fe bearing kaolinite-like minerals (Fe-Kln), red is ferric oxyhydroxide).

(E–H) BSE-SEM micrographs revealing the microstructure of the soil aggregates (Note: Fe-Si rich cements include Fe bearing kaolinite like minerals and Fe (oxy)hydroxides, as well as Fh-Si (ferrihydrite-silica co-precipitates)).

(I) EDS spectra showing the elemental composition of the selected area in "h".

(J), XRD spectra of macroaggregates (250–2000 μm) and microaggregates (53–250 μm) in soil (Qz-Quartz; Kln-Kaolinite; Hem-Hematite; No-Nontronite).

(K) *k* space Fe K-edge EXAFS spectra (weight 3) (line) and linear combination fitting (LCF, dashed) of soil aggregates. The right column shows the results of the fitting Fe K-edge EXAFS spectra. The fitting parameters: For Macro-aggregates: R factor = 0.017; Chi-square = 26.9; Reduced chi-square = 0.15; For Micro-aggregates: R factor = 0.047; Chi-square = 70.1; Reduced chi-square = 0.39.

(L) Synchrotron based C1s NEXAFS spectra of soil aggregates. Note: 1, 285.2 eV, aromatic C; 2, 286.4 eV, phenolic C; 3, 287.4 eV, alkyl C; 4, 288.4 eV, carboxyl C; 5, 289.3 eV, O-alkyl C.

(M and N), Two-dimensional NanoSIMS images for the native Fe rich soil aggregates. The red is $^{56}Fe^{16}O$, the green is ^{12}C, and the blue is $^{27}Al^{16}O$. The range of counts for these images are: $^{56}Fe^{16}O$, 0–300; ^{12}C, 0–100; $^{27}Al^{16}O$, 0–120.

These acids then initiated pH neutralization and mineral weathering and acted as organic cements for organo-mineral association.[35,36] These OC was distributed in a heterogeneous pattern, possibly because of their selective adsorption onto the Fe/Al bearing minerals, which were also randomly distributed (Figure 3).

The binding of OC compounds onto minerals under circumneutral pH conditions may have been driven by reactions between the OH groups of Fe/Al-rich minerals with carboxyl, aromatic and phenolic groups, forming polar covalent X-O-C bonds (X = Fe, Al, or Si)[37] or via hydrophobic interactions between hydrophobic organic compounds (e.g., those aromatic, and/or aliphatic dominated organics) and minerals.[38] As illustrated by the layer-by-layer model,[39] the initial association of organics with mineral surfaces functions as a nucleation site for the formation of stable aggregates.[13] However, there was no mineral cements in the adjoining spaces that connecting different mineral particles in the tailings (Figures 3D and 3F). Therefore, the aggregates were mainly supported by organic cements in the "early technosol", which we believe are transitional cements that may undergo rapid microbial decomposition, leading to aggregate dispersion.

Generation of colloidal Fe(III)-Si rich cements to enhance aggregate stability

After extensive physical, chemical and biological improvements, the resultant "early technosols" would have functions to support the growth of tolerant pioneer plants (Figure 1). All pioneer plants grew well in the "early technosol" (Figure 1), except *Sorghum* spp. that died because of the possible salt stress resulting from the extensive K dissolution; porewater K concentration increased to around 1000 mg L^{-1} (Figure S14) during initial weathering of primary minerals. The root activities of colonizing plants would subsequently enhance mineral weathering to form secondary mineral cements for the formation of a new class of more stable aggregates in emerging "advanced technosol" (Figures 2 and 4).

The microstructure within microaggregates showed that the secondary mineral phases such as irregular Fe-Si rich minerals, were generated. These, in turn, cemented quartz, biotite and FeOx particles in the "advanced technosols" after plant colonization (Figure 4), leading to the elevated stability of aggregates. These mineral cements were probably amorphous Fe(III)-Si short range ordered (SRO) minerals, which were found to be enriched in colloidal fractions within aggregates (Figure 5). It is reported that the colloidal fraction was small in size (below 1 μm) and high in chemical reactivity with other minerals and organics,[40,41] acting as an important constituent of mineral cements for forming aggregates.[42]

The Fe(III)-Si rich SRO minerals are considered to have resulted from the co-precipitation of dissolved Fe(III) and Si species (Figure 9A) generated from the weathering of primary minerals (such as biotite) in the tailings.[19,20] Typically, the Fe(II) cations liberated from weathered minerals may be rapidly oxidized to Fe(III) (Figure S8), to form Fe(III) oxyhydroxide minerals (e.g., ferrihydrite) under circumneutral pH conditions through processes like hydrolysis and polymerization.[43] The co-presence of amorphous/soluble silica hinders Fe(III) mineral polymerization, favoring the formation of Fe(III)-Si rich SRO minerals.[44] This may explain why Fe(III)-Si-SRO were so abundant in the colloidal fraction (Figure 5A). These nanosized Fe(III)-Si-SRO minerals have a high affinity for organic molecules,[45] forming close association with organics as nuclei sites to agglomerate other mineral particles (i.e., primary mineral biotite and quartz), leading to the formation of stable aggregate structure. The mixed layered minerals (e.g., illite and smectite) in the non-colloidal fractions of microaggregates (Figure S6), possibly resulting from the solid-alteration of biotite minerals in the tailings,[46] may also partially contribute to the aggregate formation.

Rhizosphere processes enhancing formation of colloidal Fe(III)-Si-SRO like minerals

Plant colonization can influence the mineralogical composition in colloidal fraction via alteration of pH, ionic strength, and/or organic groups in the tailing solutions (Figure 9). The circumneutral to slightly alkaline pH conditions (Figure S12) and the organic acid generation (Figure S13) by root activities facilitated the formation of ferrihydrite or Fe(III)-Si-SRO minerals (Figure 9A).[20] It is noted that the initial weathering of biotite like minerals and the rapid release of K and Mg into porewater elevated salinity of the tailings (Figure S14), which could hinder the Fe(III)-Si-SRO formation.[47] However, plant uptake of these elements ultimately lowered porewater ionic strength (Tables S3 and S4, Figures S12 and S14), which, in turn, would have progressively favored Fe(III)-Si-SRO formation (Figure 9B)[19,20] and diminished sylvite and aphthitalite minerals in colloidal fraction (Figure S6). In addition, the changes of composition and abundance of individual organic acids (e.g., the increase of acetic acid, Figure S13) in the rhizosphere would have enhanced mineral weathering and Fe(III)-Si-SRO formation.[48] The organic functional groups such as aromatic and/or carboxyl groups (Figure 6) may complex Fe cations to form Fe-OM complexes, as has previously been demonstrated in numerous natural and man-made environments.[49] These hindered Fe, Si and Al polymerization,[50] and facilitated the formation of SRO mineral-OM complexes (Figure 9B).[51] In sum, the association between SRO minerals and organics acts as nucleus underpinning the formation of water stable aggregates and

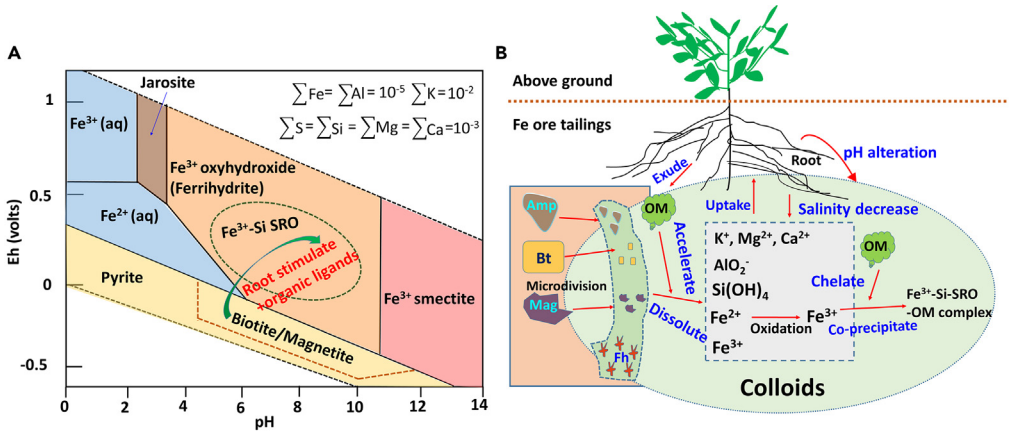

Figure 9. Diagram showing processes and possible mechanisms underlying rhizosphere driven mineral weathering and Fe(III)-Si mineral formation in Fe ore tailings

(A) Eh-pH diagram showing the key geochemical evolution pathways during pioneer plant driven secondary Fe-Si mineral (especially Fe-Si rich short range ordered (SRO) minerals) formation coupled with primary mineral weathering in the advanced technosols.

(B) Diagram summarizing plant root driven mineral weathering and secondary colloidal Fe(III)-Si-SRO-OM complex formation. The primary minerals (biotite, amphibole, magnetite) were expected to have undergone microdivision by root effects, forming micro- and nano-sized particles in colloids. These small-sized mineral particles are easily to be dissolved under functions of organic groups exuded by roots, causing the release of Fe^{2+}, Fe^{3+}, silica, and aluminum, as well as salt elements such as K^{+}, Mg^{2+} and Ca^{2+}. The salt elements were further taken up by halophyte plants, which stimulated further mineral weathering. The Fe^{2+} could be oxidized to Fe^{3+}, which would co-precipitate together with silica in the presence of organics under rhizosphere modified geochemical conditions, leading to the formation of Fe(III)-Si-SRO-OM complexes.

Note: Bt: Biotite; Amp: Amphibole; Mag: Magnetite; Fh: Ferrihydrite; OM: Organic matter; SRO: Short range ordered minerals.

organic matter stabilization,[14] both of which are fundamental and essential processes leading to soil formation in the tailings.

Rhizosphere processes may have also accelerated mineral weathering and amorphous mineral formation through stimulating key microbial development in tailings. Particularly, plant colonization increased the percentage of functional microbes involved in mineral weathering, such as Fe phyllosilicate and/or rock associated bacteria Verrucomicrobiaceae (belong to phlum Verrucomicrobia)[24] and endolithic Ellin6075 (belong to phlum Acidobacteria)[25] at family level (Figure S17), as well as *Bacillus* spp., *Helothiobacillus* spp., *Solibacillus* spp., *Streptomyces* spp., *Geobacter* spp., and *Thiobacillus* spp.[18](Table S5). These ongoing enrichment of diverse mineral associated microbes in rhizosphere further contributed to the progressive weathering of Fe bearing minerals to form increasing amounts of secondary Fe(III)-Si minerals, advancing aggregate structure development in the technosols.

Conceptual synthesis of mineral cements generation and aggregate development in tailing-soil formation

The study has demonstrated the development of stable aggregate structure in Fe ore tailings through continuous mineral weathering and amorphous Fe(III)-Si mineral formation which was driven by microbes and pioneer plant root activities. The Fe(III)-Si rich mineral cements are critical to soil aggregate stability, which was also revealed through detailed characterization of mineral makeup, distribution and organo-mineral association in native Fe rich soil (Ferralsol) aggregates from the local Fe-ore mine site (Figure 8). The Fe(III)-Si rich mineral cements in soil aggregates mostly consisted of amorphous Fe(III) oxyhydroxides and Fe(III) bearing 1: 1 aluminosilicates (kaolinite, or halloysite) (Figures 8 and S18–S20), which most likely came from the weathering of primary minerals (i.e., biotite, amphibole) with K and/or Ca depletion.[52] The isomorphic substitution of Al^{3+} by Fe^{3+} in the phyllosilicate structure could then have caused structural disorder and increased surface area and reactivity of kaolinite.[53,54] In addition, amorphous Fe(III) oxyhydroxides may have co-precipitated with secondary 1:1 phyllosilicates (e.g., via electrostatic interactions) to form "gel" like Fe(III)-rich mineral cements.[36,55] These Fe(III)-Si rich cements in soil aggregates were found to be

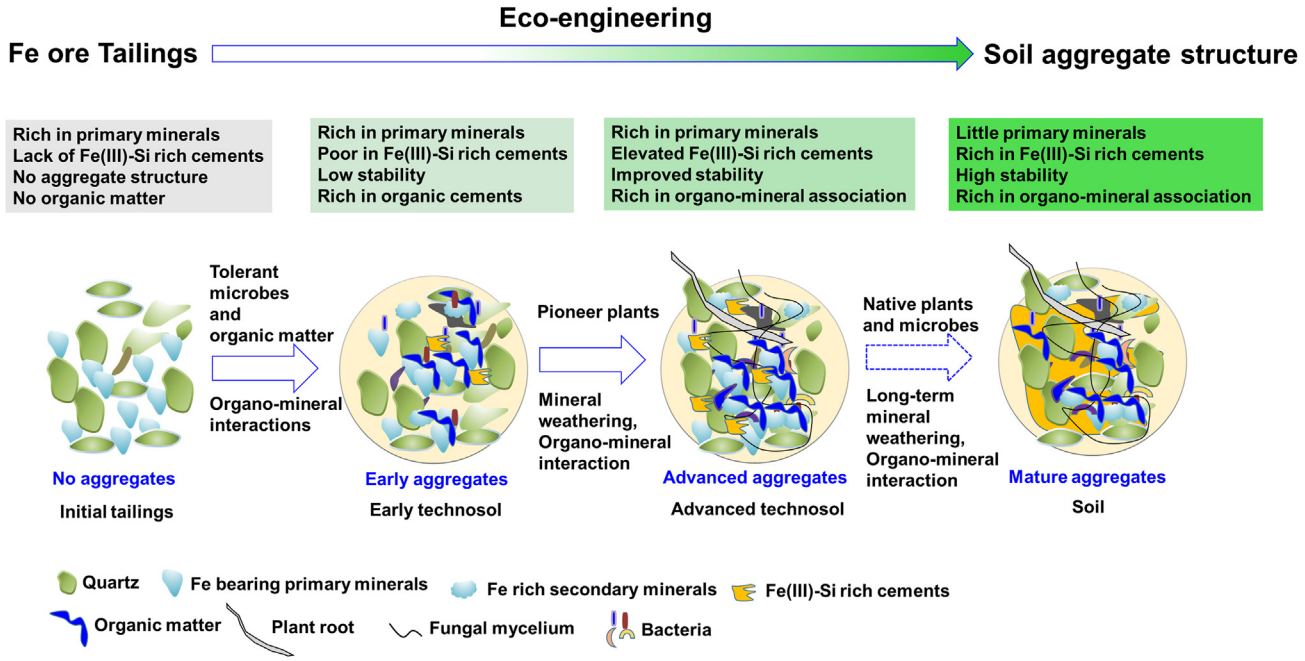

Figure 10. A conceptual model for eco-engineering stable soil aggregate structure in Fe ore tailings

The early aggregates (formed in "early technosol") could be initiated through microbial decomposition of exogenous organic matter and resultant organics cementation. The transition from early aggregates into advanced aggregates could be achieved through the accumulation of Fe(III)-Si rich cements during mineral weathering and geochemical reactions driven by intensive pioneer plant colonization. Mature aggregates can be progressively formed via long-term biotic and abiotic mediated processes of mineral weathering and Fe(III)-Si rich cements generation and accumulation, which collectively maintain the hydrological and geochemical stability of the aggregates.

mostly in the colloidal fraction (Figure S23), which not only confer strong physical stability, but also provide affinitive surfaces for interactions with carboxylic dominated organics (Figure 8L), underpinning organo-mineral association and nucleation sites for aggregate structure development.[39]

However, it is important to point out that the proportion of colloidal Fe(III)-Si rich cements in aggregates in the "advanced technosol" (0.4–0.8% w/w) remained much lower than those of native soil aggregates (3.5% w/w). This difference may explain the lower stability of the technosol aggregates than that of native soil aggregates. The aggregate structure and stability development in the tailings may be enhanced by increasing the generation of Fe(III)-Si cements during the eco-engineering processes and the technosol development over the time. From the perspective of natural pedogenetic processes, Fe(III)-Si rich mineral cements in soil aggregates should have formed via the long-term primary mineral weathering driven by continuous plant root and microbial activities.[52] A conceptual model has thus been proposed to demonstrate procedures of aggregate development in the tailings (Figure 10).

Briefly, the initial aggregates in "early technosol" can be formed through cementing effects of organic materials derived from microbial OM decomposition, which intimately associate with tailing minerals. The aggregates are progressively consolidated by accumulating Fe(III)-Si rich mineral cements generated from the weathering of primary minerals (such as biotite) and the formation of colloidal Fe(III)-Si short range ordered (SRO) minerals, which are stimulated by ongoing rhizosphere activities of tolerant plants in the developing technosol. Those colloidal Fe(III)-Si SRO minerals would be polymerized into ferrihydrite-Si, goethite and even hematite, during long-term aging. These more stable secondary minerals together with Fe(III)-Si SRO minerals would form new Fe(III)-Si rich mineral cements, serving as reactive sites for association with other mineral particles and organics to enhance aggregate stability under the semi-arid climatic conditions (Figure 10). The development of soil aggregate structure in "advanced technosol" subsequently facilitates the colonization of various plant/microbial communities, from pioneer plant species to diverse keystone plant species, in association with key soil microbes such as mycorrhizal fungi.[56] These plant and rhizosphere microbial activities in the tailings would consistently stimulate the long-term soil aggregate development, through enhancing mineral weathering, Fe(III)-Si rich cements formation and

organic matter stabilization (Figure 10). This would lead to a quasi-stable soil-like substrate, with strong and mature aggregate structure for supporting long-term resilient revegetation and ecosystem build-up in the tailing sites.

It is important to point out that we have emphasized the key role of bioweathering and secondary Fe(III)-Si mineral cements in the formation of stable soil aggregate structure in Fe ore tailings undergoing soil formation. These secondary Fe(III)-Si minerals in the microaggregates significantly increase OC sequestration, because of their high reactivity and specific surface area.[41] These organo-mineral complexes embedded in microaggregates contribute to the long-term retention of OC.[14] The organo-mineral association formed through interactions of these secondary Fe(III)-Si minerals with functional organics are of critical importance to not only soil structure development, but also the development of biogeochemical functions in the technosols for resilient ecological rehabilitation of tailings landscapes.[57] We have demonstrated the approach to harness biological drivers of tolerant microbes and pioneer native plants as the key soil formation factors in accelerating critical processes of bio-generation of mineral cements (i.e., amorphous Fe(III)-Si minerals) and formation of microaggregates. This process is the key to unlock the barrier to soil formation in the mechanically compacted tailings without functional physical structure.

Ecological rehabilitation of large areas of Fe-ore tailings landscapes worldwide requires large volumes of natural soils by excavating natural landscapes, which is not a sustainable option. Our findings have opened a cost-effective and sustainable pathway to achieve ecological rehabilitation of Fe-ore tailings without natural soil, potentially solving the big environmental issues of thousands of hectares of mine tailing sites globally. The merits of environmental and economic sustainability lie in the fact that our approach to eco-engineer tailings into functional soil for supporting revegetation does not require the supply of many millions of cubic meters of natural soil at mine sites for rehabilitating hundreds to thousands of ha of tailings landscape. Furthermore, the access to natural soil supply is beyond the reach of many mine sites, regardless of financial capability. Compared to conventional method by relying on excavated topsoil to construct soil cover, the rehabilitation of Fe ore tailings through the proposed eco-engineering pathway has been estimated to save up to 50–70% of the rehabilitation costs. For instance, in Australia, the current price of natural soil supply from offsite ranges is from \$30 to 120/m^3, including handling and transport expenses, which is translated to the cost of \$300,000–1,200,000 per ha if using natural soil to create 1 m soil cover across a tailings landscape. As a result, the translation of this eco-engineering approach in field operations would lead to rapid rehabilitation progress and potential savings worth many billions of dollars, if adopted across the thousands ha of Fe ore mine tailings landscapes worldwide.

Our work has proved the concept of eco-engineering of Fe ore tailings into soil-like technosol through a pot experiment under glasshouse conditions. Soil aggregate structure were formed and progressively developed in tailings to support soil functionality during eco-engineering processes driven by tolerant microbial community and pioneer plants. The initial aggregates in "early technosol" contained little Fe(III)-Si cements and were mainly held together by organic cements. Later, rhizosphere biogeochemical processes of pioneer plants induced the generation of colloidal Fe(III)-Si SRO minerals, which sequestrated organic carbon and consolidated the aggregate structure and stability. The importance of Fe(III)-Si rich cements in underpinning aggregate structure was confirmed in native Fe rich soil surrounding the investigated tailing site. Based on these findings, we propose a conceptual model for progressive aggregate structure development in the tailings with Fe(III)-Si rich cements as core nuclei. The eco-engineering process proposed here can be tailored for local resource availability and climatic conditions in future scale-up field trials before adoption at remote mine sites.

Limitations of the study

In this study, we have demonstrated the approach to employ tolerant microbes and pioneer plants as the key drivers in accelerating *in situ* mineral weathering and secondary mineral cement formation for aggregate development toward eco-engineered soil formation in Fe ore tailings. The concept has been proved under the short-term glasshouse conditions. However, it is essential to scale up the proof of concept into the operational methodology by conducting long-term broadacre field trials at Fe ore tailings landscape, with consideration of climate and parent material variability across spatial distance and different field operators. Furthermore, because this study was only carried out using the magnetite alkaline Fe ore tailings as an example, it is necessary to investigate the suitability of this approach in eco-engineering soil formation in other tailings, such as hematite Fe ore tailings and Cu tailings.

STAR★METHODS

Detailed methods are provided in the online version of this paper and include the following:

SUPPLEMENTAL INFORMATION

Supplemental information can be found online at https://doi.org/10.1016/j.isci.2023.107102.

ACKNOWLEDGMENTS

The work is financially supported by Australian Research Council Linkage Project (LP160100598), Karara Mining limited, and The Botanic Gardens and Parks Authority (BGPA). S. Wu also acknowledges the UQECR funding (613767). XFM mapping was undertaken on the XFM beamline at the Australian Synchrotron, part of ANSTO (AS182/XFM/13331). The XAS analysis was undertaken on the XAS beamline at the Australian Synchrotron, part of ANSTO (Project Reference No: AS191/XAS/14392), as well as 01C1, 17C1 and 20A1 beamline in National Synchrotron Radiation Research Centre (NSRRC), Taiwan. The authors also thank Dr Jin-Ming Chen in Beamline 20A1 and Dr Jyh-Fu Lee in beamline 17C1, NSRRC, Taiwan for technical support in XAS analysis. Dr Jeremy Wykes at XAS beamline of Australian synchrotron is also acknowledged for technical support in XAS analysis. NanoSIMS analysis was done at Center for Microscopy, Characterization and Analysis at University of Western Australia. The authors acknowledge staffs in Australian Microscopy & Microanalysis Research Facility at the Center for Microscopy and Microanalysis, The University of Queensland for assistance in XRD, XPS and BSE-SEM-EDS analysis. The Australian Center for Ecogenomics, the University of Queensland, Australia was acknowledged for Illumina sequencing analysis. Dr Elaine Wrightman in JKMRC, SMI, UQ has been acknowledged for support in MLA analysis. We also thank Dr Shuncai Wang and Jingfang Xue for help on the plant cultivation, maintenance, and harvest, as well as lab analysis.

AUTHOR CONTRIBUTIONS

S.W.: Conceptualization, Experimental design and conduction, Methodology, Data analysis, Writing-original draft, and review & editing; Y.L.: Methodology (Plant harvest, XFM analysis); Z.L., L.R., and Q.Y.: Methodology (Plant harvest, wet sieving); F.Y.: Methodology (Microbial community analysis); J.J.B.: Methodology (NanoSIMS analysis); D.P.: Methodology (XFM analysis); S.C.H.: Methodology (C 1s NEXAFS analysis); T.S.C. and Y.R.L.: Methodology (Fe K edge XAFS analysis); M.H. and N. S.: Methodology (ICP-OES analysis); G.S., K.K., T.N., and Y.S.O.: Writing-review & editing; L.H.: Conceptualization, Experimental design, Project administration, Funding acquisition, Writing-review & editing.

DECLARATION OF INTERESTS

The authors declare no competing interests.

INCLUSION AND DIVERSITY

We support inclusive, diverse, and equitable conduct of research.

Received: January 19, 2023
Revised: March 20, 2023
Accepted: June 8, 2023
Published: June 24, 2023

REFERENCES

1. Mudd, G.M. (2010). The environmental sustainability of mining in Australia: key mega-trends and looming constraints. Resour. Pol. *35*, 98–115.

2. Lottermoser, B. (2010). Tailings, Mine Wastes (Springer Berlin Heidelberg), pp. 205–241.

3. Hudson-Edwards, K. (2016). Tackling mine wastes. Tackling mine wastes *352*, 288–290.

4. Franks, D.M., Stringer, M., Torres-Cruz, L.A., Baker, E., Valenta, R., Thygesen, K., Matthews, A., Howchin, J., and Barrie, S. (2021). Tailings facility disclosures reveal stability risks. Sci. Rep. *11*, 5353. https://doi.org/10.1038/s41598-021-84897-0.

5. Franks, D.M., Stringer, M., Baker, E., Valenta, Rick, Torres-Cruz, L.A., Thygesen, K., Matthews, A., Howchin, J., and Barrie, S. (2020). Lessons from Tailings Facility Data Disclosures. In Towards Zero Harm: A Compendium of Papers Prepared for the Global Tailings Review, B. Oberle, D. Brereton, and A. Mihaylova, eds., pp. 84–108.

6. Carmignano, O., Vieira, S., Teixeira, A.P., Lameiras, F., Brandão, P.R., and Lago, R. (2021). Iron Ore Tailings: Characterization and Applications. J. Braz. Chem. Soc. https://doi.org/10.21577/0103-5053.20210100.

7. Wu, S., Liu, Y., Southam, G., Robertson, L., Chiu, T.H., Cross, A.T., Dixon, K.W., Stevens, J.C., Zhong, H., Chan, T.-S., et al. (2019). Geochemical and mineralogical constraints in iron ore tailings limit soil formation for direct phytostabilization. Sci. Total Environ. *651*, 192–202.

8. Huang, L., Baumgartl, T., and Mulligan, D. (2012). Is rhizosphere remediation sufficient for sustainable revegetation of mine tailings? Ann. Bot. *110*, 223–238. https://doi.org/10.1093/aob/mcs115.

9. Huang, L., Baumgartl, T., Zhou, L., and Mulligan, D. (2014). The New Paradigm for Phytostabilising Mine Wastes–Ecologically Engineered Pedogenesis and Functional Root Zones (AUSIMM)), pp. 663–674.

10. Wu, S., Nguyen, T.A., Liu, Y., Southam, G., Wang, S., Chan, T.-S., Lu, Y.-R., and Huang, L. (2019). Deficiencies of secondary Fe (oxy) hydroxides associated with phyllosilicates and organic carbon limit the formation of water-stable aggregates in Fe-ore tailings. Chem. Geol. *523*, 73–87. https://doi.org/10.1016/j.chemgeo.2019.06.002.

11. Amézketa, E. (1999). Soil Aggregate Stability: A Review. J. Sustain. Agric. *14*, 83–151. https://doi.org/10.1300/J064v14n02_08.

12. Rabot, E., Wiesmeier, M., Schlüter, S., and Vogel, H.J. (2018). Soil structure as an indicator of soil functions: A review. Geoderma *314*, 122–137. https://doi.org/10.1016/j.geoderma.2017.11.009.

13. Tisdall, J.M., and Oades, J.M. (1982). Organic matter and water-stable aggregates in soils. Eur. J. Soil Sci. *33*, 141–163.

14. Totsche, K.U., Amelung, W., Gerzabek, M.H., Guggenberger, G., Klumpp, E., Knief, C., Lehndorff, E., Mikutta, R., Peth, S., Prechtel, A., et al. (2018). Microaggregates in soils. J. Plant Nutr. Soil Sci. *181*, 104–136.

15. Duiker, S.W., Rhoton, F.E., Torrent, J., Smeck, N.E., and Lal, R. (2003). Iron (hydr) oxide crystallinity effects on soil aggregation. Soil Sci. Soc. Am. J. *67*, 606–611.

16. Lima, J.M., and Anderson, S.J. (1997). Aggregation and Aggregate Size Effects on Extractable Iron and Aluminum in Two Hapludoxs. Soil Sci. Soc. Am. J. *61*, 965–970. https://doi.org/10.2136/sssaj1997.03615995006100030036x.

17. Kelly, E.F., Chadwick, O.A., and Hilinski, T.E. (1998). The Effect of Plants on Mineral Weathering. Biogeochemistry *42*, 21–53. https://doi.org/10.1023/a:1005919306687.

18. Uroz, S., Calvaruso, C., Turpault, M.P., and Frey-Klett, P. (2009). Mineral weathering by bacteria: ecology, actors and mechanisms. Trends Microbiol. *17*, 378–387. https://doi.org/10.1016/j.tim.2009.05.004.

19. Wu, S., Liu, Y., Southam, G., Robertson, L.M., Wykes, J., Yi, Q., Hall, M., Li, Z., Sun, Q., Saha, N., et al. (2021). Rhizosphere Drives Biotite-Like Mineral Weathering and Secondary Fe–Si Mineral Formation in Fe Ore Tailings. ACS Earth Space Chem. *5*, 618–631. https://doi.org/10.1021/acsearthspacechem.0c00331.

20. Tamrat, W.Z., Rose, J., Grauby, O., Doelsch, E., Levard, C., Chaurand, P., and Basile-Doelsch, I. (2018). Composition and molecular scale structure of nanophases formed by precipitation of biotite weathering products. Geochem. Cosmochim. Acta *229*, 53–64.

21. Robertson, L.M., Wu, S., You, F., Huang, L., Southam, G., Chan, T.-S., Lu, Y.-R., and Bond, P.L. (2020). Geochemical and mineralogical changes in magnetite Fe-ore tailings induced by biomass organic matter amendment. Sci. Total Environ. *724*, 138196.

22. Nemati, M.R., Caron, J., and Gallichand, J. (2002). Predicting hydraulic conductivity changes from aggregate mean weight diameter. Water Resour. Res. *38*, 9-1–9-11.

23. Artz, R.R., Chapman, S.J., Jean Robertson, A.H., Potts, J.M., Laggoun-Défarge, F., Gogo, S., Comont, L., Disnar, J.-R., and Francez, A.-J. (2008). FTIR spectroscopy can be used as a screening tool for organic matter quality in regenerating cutover peatlands. Soil Biol. Biochem. *40*, 515–527. https://doi.org/10.1016/j.soilbio.2007.09.019.

24. Ahmed, E., Hugerth, L.W., Logue, J.B., Brüchert, V., Andersson, A.F., and Holmström, S.J.M. (2016). Mineral Type Structures Soil Microbial Communities. Geomicrobiol. J. *34*, 538–545. https://doi.org/10.1080/01490451.2016.1225868.

25. Cirigliano, A., Mura, F., Cecchini, A., Tomassetti, M.C., Maras, D.F., Di Paola, M., Meriggi, N., Cavalieri, D., Negri, R., Quagliariello, A., et al. (2020). Active microbial ecosystem in Iron-Age tombs of the Etruscan civilization. Environ. Microbiol. *23*, 3957–3969.

26. Jayamani, I., and Cupples, A.M. (2015). Stable isotope probing and high-throughput sequencing implicate Xanthomonadaceae and Rhodocyclaceae in ethylbenzene degradation. Environ. Eng. Sci. *32*, 240–249.

27. Lepleux, C., Turpault, M.P., Oger, P., Frey-Klett, P., and Uroz, S. (2012). Correlation of the abundance of betaproteobacteria on mineral surfaces with mineral weathering in forest soils. Appl. Environ. Microbiol. *78*, 7114–7119.

28. Jenny, H. (1994). Factors of Soil Formation: A System of Quantitative Pedology (Courier Corporation)).

29. Wu, S., Liu, Y., Bougoure, J.J., Southam, G., Chan, T.-S., Lu, Y.-R., Haw, S.-C., Nguyen, T.A.H., You, F., and Huang, L. (2019). Organic Matter Amendment and Plant Colonization Drive Mineral Weathering, Organic Carbon Sequestration, and Water-Stable Aggregation in Magnetite Fe Ore Tailings. Environ. Sci. Technol. *53*, 13720–13731.

30. Banfield, J.F., Barker, W.W., Welch, S.A., and Taunton, A. (1999). Biological impact on mineral dissolution: application of the lichen model to understanding mineral weathering in the rhizosphere. Proc. Natl. Acad. Sci. USA *96*, 3404–3411.

31. Angers, D.A., and Caron, J. (1998). Plant-induced changes in soil structure: processes and feedbacks. Biogeochemistry *42*, 55–72.

32. You, F., Dalal, R., and Huang, L. (2018). Biochar and biomass organic amendments shaped different dominance of lithoautotrophs and organoheterotrophs in microbial communities colonizing neutral copper(Cu)-molybdenum(Mo)-gold(Au) tailings. Geoderma *309*, 100–110. https://doi.org/10.1016/j.geoderma.2017.09.010.

33. Kersters, K., De Vos, P., Gillis, M., Swings, J., Vandamme, P., and Stackebrandt, E. (2006). Introduction to the Proteobacteria. In The Prokaryotes: Volume 5: Proteobacteria: Alpha and Beta Subclasses, M. Dworkin, S. Falkow, E. Rosenberg, K.-H. Schleifer, and E. Stackebrandt, eds. (Springer New York), pp. 3–37. https://doi.org/10.1007/0-387-30745-1_1.

34. Kalbitz, K., Schwesig, D., Schmerwitz, J., Kaiser, K., Haumaier, L., Glaser, B., Ellerbrock, R., Leinweber, P., and Biochemistry. (2003). Changes in properties of soil-derived dissolved organic matter induced by biodegradation *35*, 1129–1142.

35. You, F., Zhang, L., Ye, J., and Huang, L. (2019). Microbial decomposition of biomass residues mitigated hydrogeochemical dynamics in strongly alkaline bauxite residues. Sci. Total Environ. *663*, 216–226. https://doi.org/10.1016/j.scitotenv.2019.01.317.

36. Tombácz, E., Libor, Z., Illés, E., Majzik, A., and Klumpp, E. (2004). The role of reactive surface sites and complexation by humic acids in the interaction of clay mineral and iron oxide particles. Org. Geochem. *35*, 257–267. https://doi.org/10.1016/j.orggeochem.2003.11.002.

37. Kleber, M., Eusterhues, K., Keiluweit, M., Mikutta, C., Mikutta, R., and Nico, P.S. (2015). Mineral–Organic Associations: Formation, Properties, and Relevance in Soil Environments. Adv. Agron. *130*, 1–140. https://doi.org/10.1016/bs.agron.2014.10.005.

38. Carmo, A.M., Hundal, L.S., and Thompson, M.L. (2000). Sorption of hydrophobic organic compounds by soil materials: application of unit equivalent Freundlich coefficients. Environ. Sci. Technol. *34*, 4363–4369.

39. Chassé, A.W., Ohno, T., Higgins, S.R., Amirbahman, A., Yildirim, N., and Parr, T.B. (2015). Chemical force spectroscopy evidence supporting the layer-by-layer model of organic matter binding to iron (oxy) hydroxide mineral surfaces. Environ. Sci. Technol. *49*, 9733–9741.

40. Kretzschmar, R. (2005). COLLOID-FACILITATED SORPTION AND TRANSPORT. In Encyclopedia of Soils in the Environment, D. Hillel, ed. (Elsevier), pp. 276–284. https://doi.org/10.1016/B0-12-348530-4/00201-0.

41. Krause, L., Klumpp, E., Nofz, I., Missong, A., Amelung, W., and Siebers, N. (2020). Colloidal iron and organic carbon control soil aggregate formation and stability in arable Luvisols. Geoderma *374*, 114421. https://doi.org/10.1016/j.geoderma.2020.114421.

42. De Boodt, M.F., Hayes, M.H., and Herbillon, A. (2013). Soil Colloids and Their Associations in Aggregates (Springer Science & Business Media).

43. Schwertmann, H.C.U., and Cornell, R.M. (2000). Iron Oxides in the Laboratory: Preparation and Characterization. Clay Miner. *27*, 393.

44. Doelsch, E., Stone, W.E.E., Petit, S., Masion, A., Rose, J., Bottero, J.-Y., and Nahon, D. (2001). Speciation and crystal chemistry of Fe (III) chloride hydrolyzed in the presence of SiO4 ligands. 2. Characterization of Si− Fe aggregates by FTIR and 29Si Solid-State NMR. Langmuir *17*, 1399–1405.

45. Chen, K.Y., Chen, T.Y., Chan, Y.T., Cheng, C.Y., Tzou, Y.M., Liu, Y.T., and Teah, H.Y. (2016). Stabilization of Natural Organic Matter by Short-Range-Order Iron Hydroxides. Environ. Sci. Technol. *50*, 12612–12620. https://doi.org/10.1021/acs.est.6b02793.

46. Murakami, T., Utsunomiya, S., Yokoyama, T., and Kasama, T. (2003). Biotite dissolution processes and mechanisms in the laboratory and in nature: Early stage weathering environment and vermiculitization. Am. Mineral. *88*, 377–386.

47. Pensini, E., Sleep, B.E., Yip, C.M., O'Carroll, D.J.E.s., and technology. (2012). Forces of interactions between bare and polymer-coated iron and silica: Effect of ph, ionic strength, and humic acids. Environ. Sci. Technol. *46*, 13401–13408.

48. Bray, A.W., Oelkers, E.H., Bonneville, S., Wolff-Boenisch, D., Potts, N.J., Fones, G., and Benning, L.G. (2015). The effect of pH, grain size, and organic ligands on biotite weathering rates. Geochem. Cosmochim. Acta *164*, 127–145. https://doi.org/10.1016/j.gca.2015.04.048.

49. Konhauser, K., and Riding, R. (2012). Bacterial biomineralization. Fundamentals of geobiology, 105–130.

50. Chen, K.-Y., Chen, T.-Y., Chan, Y.-T., Cheng, C.-Y., Tzou, Y.-M., Liu, Y.-T., Teah, H.Y., and technology. (2016). Stabilization of natural organic matter by short-range-order iron hydroxides. Environ. Sci. Technol. *50*, 12612–12620.

51. Tamrat, W.Z., Rose, J., Grauby, O., Doelsch, E., Levard, C., Chaurand, P., and Basile-Doelsch, I. (2019). Soil organo-mineral associations formed by co-precipitation of Fe, Si and Al in presence of organic ligands. Geochem. Cosmochim. Acta *260*, 15–28.

52. Velde, B.B., and Meunier, A. (2008). The Origin of Clay Minerals in Soils and Weathered Rocks (Springer Science & Business Media).

53. Malden, P.J., and Meads, R.E. (1967). Substitution by Iron in Kaolinite. Nature *215*, 844–846. https://doi.org/10.1038/215844b0.

54. Gidigasu, M. (2012). Laterite Soil Engineering: Pedogenesis and Engineering Principles (Elsevier).

55. Johnston, C.T., and Tombacz, E. (2002). Surface Chemistry of Soil Minerals (Soil mineralogy with environmental applications), pp. 37–67.

56. Li, Z., Wu, S., Liu, Y., Yi, Q., You, F., Ma, Y., Thomsen, L., Chan, T.-S., Lu, Y.-R., Hall, M., et al. (2022). Arbuscular mycorrhizal symbiosis enhances water stable aggregate formation and organic matter stabilization in Fe ore tailings. Geoderma *406*, 115528. https://doi.org/10.1016/j.geoderma.2021.115528.

57. Kögel-Knabner, I., Guggenberger, G., Kleber, M., Kandeler, E., Kalbitz, K., Scheu, S., Eusterhues, K., and Leinweber, P. (2008). Organo-mineral associations in temperate soils: Integrating biology, mineralogy, and organic matter chemistry. J. Plant Nutr. Soil Sci. *171*, 61–82. https://doi.org/10.1002/jpln.200700048.

58. Huang, C.Y.L., and Schulte, E.E. (1985). Digestion of plant tissue for analysis by ICP emission spectroscopy. Commun. Soil Sci. Plant Anal. *16*, 943–958. https://doi.org/10.1080/00103628509367657.

59. You, F., Dalal, R., Mulligan, D., and Huang, L. (2015). Quantitative Measurement of Organic Carbon in Mine Wastes: Methods Comparison for Inorganic Carbon Removal and Organic Carbon Recovery. Commun. Soil Sci. Plant Anal. *46*, 375–389. https://doi.org/10.1080/00103624.2014.989113.

60. Rayment, G.E., and Lyons, D.J. (2011). Soil Chemical Methods: Australasia (CSIRO publishing).

61. Caporaso, J.G., Lauber, C.L., Walters, W.A., Berg-Lyons, D., Huntley, J., Fierer, N., Owens, S.M., Betley, J., Fraser, L., Bauer, M., et al. (2012). Ultra-high-throughput microbial community analysis on the Illumina HiSeq and MiSeq platforms. ISME J. *6*, 1621–1624.

62. Cayford, B.I., Dennis, P.G., Keller, J., Tyson, G.W., and Bond, P.L. (2012). High-throughput amplicon sequencing reveals distinct communities within a corroding concrete sewer system. Appl. Environ. Microbiol. *78*, 7160–7162.

63. Bolyen, E., Rideout, J.R., Dillon, M.R., Bokulich, N.A., Abnet, C.C., Al-Ghalith, G.A., Alexander, H., Alm, E.J., Arumugam, M., Asnicar, F., et al. (2019). Reproducible, interactive, scalable and extensible microbiome data science using QIIME 2. Nat. Biotechnol. *37*, 852–857.

64. Martin, M. (2011). Cutadapt removes adapter sequences from high-throughput sequencing reads. EMBnet. j. *17*, 10–12.

65. Amir, A., McDonald, D., Navas-Molina, J.A., Kopylova, E., Morton, J.T., Zech Xu, Z., Kightley, E.P., Thompson, L.R., Hyde, E.R., Gonzalez, A., and Knight, R. (2017). Deblur rapidly resolves single-nucleotide community sequence patterns. mSystems *2*, e00191-16–e00116.

66. Oksanen, J., Kindt, R., Legendre, P., O'Hara, B., Stevens, M.H.H., Oksanen, M.J., and Suggests, M. (2007). The vegan package. Community ecology package *10*, 631–637.

67. Clarke, K.R. (1993). Non-parametric multivariate analyses of changes in community structure. Austral Ecol. *18*, 117–143.

68. Kemper, W., and Rosenau, R. (1986). Aggregate stability and size distribution. In Methods of Soil Analysis, Part 1: Physical and MineralogicalMethods, Klute, ed. (Soil Science Society of America), pp. 425–442.

69. Schumacher, M., Christl, I., Scheinost, A.C., Jacobsen, C., and Kretzschmar, R. (2005). Chemical Heterogeneity of Organic Soil Colloids Investigated by Scanning Transmission X-ray Microscopy and C-1s NEXAFS Microspectroscopy. Environ. Sci. Technol. *39*, 9094–9100. https://doi.org/10.1021/es050099f.

70. Pokrovski, G.S., Schott, J., Farges, F., and Hazemann, J.-L. (2003). Iron (III)-silica interactions in aqueous solution: Insights from X-ray absorption fine structure spectroscopy. Geochem. Cosmochim. Acta *67*, 3559–3573.

71. Ravel, B., and Newville, M. (2005). ATHENA, ARTEMIS, HEPHAESTUS: data analysis for

X-ray absorption spectroscopy using IFEFFIT. J. Synchrotron Radiat. *12*, 537–541.

72. Solomon, D., Lehmann, J., Kinyangi, J., Liang, B., and Schäfer, T. (2005). Carbon K-edge NEXAFS and FTIR-ATR spectroscopic investigation of organic carbon speciation in soils. Soil Sci. Soc. Am. J. *69*, 107–119.

73. Prietzel, J., Müller, S., Kögel-Knabner, I., Thieme, J., Jaye, C., and Fischer, D. (2018). Comparison of soil organic carbon speciation using C NEXAFS and CPMAS 13 C NMR spectroscopy. Sci. Total Environ. *628–629*, 906–918.

74. Steffens, M., Rogge, D.M., Mueller, C.W., Höschen, C., Lugmeier, J., Kölbl, A., and Kögel-Knabner, I. (2017). Identification of Distinct Functional Microstructural Domains Controlling C Storage in Soil. Environ. Sci. Technol. *51*, 12182–12189. https://doi.org/10.1021/acs.est.7b03715.

75. Paterson, D., De Jonge, M., Howard, D., Lewis, W., McKinlay, J., Starritt, A., Kusel, M., Ryan, C., Kirkham, R., and Moorhead, G. (2011). In The X-ray Fluorescence Microscopy Beamline at the Australian Synchrotron, *1*The X-ray Fluorescence Microscopy Beamline at the Australian Synchrotron (AIP)), pp. 219–222.

76. Kirkham, R., Dunn, P., Kuczewski, A., Siddons, D., Dodanwela, R., Moorhead, G., Ryan, C., De Geronimo, G., Beuttenmuller, R., and Pinelli, D. (2010). In The Maia Spectroscopy Detector System: Engineering for Integrated Pulse Capture, Low-latency Scanning and Real-time Processing, *1*The Maia Spectroscopy Detector System: Engineering for Integrated Pulse Capture, Low-latency Scanning and Real-time Processing (AIP)), pp. 240–243.

77. Ryan, C., Etschmann, B., Vogt, S., Maser, J., Harland, C., Van Achterbergh, E., and Legnini, D. (2005). Nuclear microprobe–synchrotron synergy: Towards integrated quantitative real-time elemental imaging using PIXE and SXRF. Nucl. Instrum. Methods Phys. Res. Sect. B Beam Interact. Mater. Atoms *231*, 183–188.

78. Fandrich, R., Gu, Y., Burrows, D., and Moeller, K. (2007). Modern SEM-based mineral liberation analysis. Int. J. Miner. Process. *84*, 310–320.

79. Kopittke, P.M., Hernandez-Soriano, M.C., Dalal, R.C., Finn, D., Menzies, N.W., Hoeschen, C., and Mueller, C.W. (2018). Nitrogen-rich microbial products provide new organo-mineral associations for the stabilization of soil organic matter. Global Change Biol. *24*, 1762–1770.

STAR★METHODS

KEY RESOURCES TABLE

REAGENT or RESOURCE	SOURCE	IDENTIFIER
Biological samples		
Atriplex amnicola	Nindethana Ltd., Australia	N/A
Maireana brevifolia	Nindethana Ltd., Australia	N/A
Sorghum spp. Hybrid cv. Silk	Pukalus's farm in Injune origin, Queensland, Australia	N/A
Chemicals, peptides, and recombinant proteins		
Magnetite iron ore tailings	Karara Mining Ltd	N/A
Hematite	Sigma Aldrich	CAS ID: 1317-60-8
Goethite	Sigma Aldrich	CAS ID: 20344-49-4
Magnetite	Sigma Aldrich	CAS ID: 7439-89-6
Siderite	Sigma Aldrich	CAS ID: 14476-16-5
Pyrite	Sigma Aldrich	CAS ID: 1309-36-0
Fe(III)-citrate	Sigma Aldrich	CAS ID: 3522-50-7
Fe(II)-gluconate hydrate	Sigma Aldrich	CAS ID: 699014-53-4
Fe(II)-oxide	Sigma Aldrich	CAS ID: 1345-25-1
Jarosite	Sigma Aldrich	CAS ID: 12207-14-6
Fe(III)-sulfate	Sigma Aldrich	CAS ID: 10028-22-5
Iron(III)-nitrate	Sigma Aldrich	CAS ID: 7782-61-8
Sodium silicate	Sigma Aldrich	CAS ID.: 6834-92-0
Oxalic acid	Sigma Aldrich	CAS ID: 144-62-7
Illite	Ward's science	https://www.wardsci.com
Vermiculite	Ward's science	https://www.wardsci.com
Epidote	Ward's science	https://www.wardsci.com
Biotite	Ward's science	https://www.wardsci.com
Olivine	Ward's science	https://www.wardsci.com
Critical commercial assays		
DNeasy PowerSoil Kit	QIAGEN	https://www.qiagen.com/au/
Oligonucleotides		
926F (5′-AAACTYAAAKGAATTGACGG-3′)	Australian Centre for Ecogenomics, the University of Queensland	N/A
1392wR (5′-ACGGGCGGTGWGTRC-3′)	Australian Centre for Ecogenomics, the University of Queensland	N/A
Software and algorithms		
QIIME2 (Quantitative Insights Into Microbial Ecology 2, version 2019.1)	QIIME 2 development team	https://qiime2.org/
SPSS statistics 18	IBM	https://www.ibm.com/
Origin 2021	OriginLab	https://www.originlab.com/
Excel	Microsoft	https://www.microsoft.com/
R (v3.4.1)	R Project	https://cran.r-project.org/
Diffracplus Evaluation Package V4.2	Bruker AXS, Germany	https://www.bruker.com/
DEMETER software package	CARS, University of Chicago	https://bruceravel.github.io/demeter/
GeoPIXE	CSIRO, Australia	http://nmp.csiro.au/geopixe.html

(*Continued on next page*)

Continued

REAGENT or RESOURCE	SOURCE	IDENTIFIER
OpenMIMS data analysis software	National Resource for Imaging Mass Spectrometry	http://nrims.harvard.edu
CasaXPS software package	Casa Software Ltd	http://www.casaxps.com/
ImageJ	National Institutes of Health, Bethesda, MD, USA	https://imagej.nih.gov/ij/
CANOCO 5.0	Microcomputer Power, Ithaca, NY, USA	http://www.canoco5.com/
Other		
FRITSCH Analysette 3-laboratory model of vibration sifting device	Fritsch, Germany	https://www.fritsch-international.com/
Cary 630 FTIR with Diamond ATR module	Agilent Technologies, Palo Alto, CA, USA	https://www.agilent.com/
Hitachi SU3500 SEM	Hitachi, Japan	https://www.hitachi-hightech.com/
Copper grid (200 mesh)	ProSciTech Pty. Ltd., Queensland, Australia	https://proscitech.com.au/
NanoSIMS 50L	Cameca, Gennevilliers, France	https://www.cameca.com/products/sims/nanosims
Hitachi HF5000 S/TEM	Hitachi, Japan	https://www.hitachi-hightech.com/

RESOURCE AVAILABILITY

Lead contact

Further information and requests for resources should be directed to the lead contact, Longbin Huang (Email: l.huang@uq.edu.au)

Materials availability

All materials used in this study are available from the lead contact upon reasonable request.

Data and code availability

- All data that support the findings in this study are available in the article and its supplemental information.
- This study did not generate original code.
- Any additional information required to reanalyze the data reported in this work is available from the lead contact upon reasonable request.

METHOD DETAILS

Experimental procedures

Tailings and soil collection

The Fe-ore tailings was collected from the tailings dam (GPS: 29.19842°S 116.75972°E) within a magnetite Fe-ore mine site in Western Australia, which was rich in biotite mica, quartz, Fe(III) oxyhydroxides (described previously[7,29]) (Figure S24). The tailings were strongly alkaline (pH 9.5), with low level of organic carbon (0.1% w/w) and nitrogen (0.1% w/w), but high amount of quartz and primary phyllosilicate (biotite-like) in the form of fine particles (below 53 μm, with little water stable aggregate structure).[7] Native Fe-rich soils were collected from a natural undisturbed site adjacent to the investigated Fe ore mine site in Western Australia (GPS: 29.19717° S, 116.76222° E) (Figure S24). The soil had a neutral pH, with 0.6% w/w organic carbon and 0.6% w/w nitrogen, with abundant kaolinite, quartz and hematite and Fe hydroxides (e.g. goethite, ferrihydrite) and well water stable aggregates.[7] The details of the physical and chemical properties of initial tailings and native Fe rich soils are in Table S1. As the soils were collected from the sorrounding area of the tailing site, the comparation is reasonable.

Eco-engineering of the tailings

In "*early technosol" formation process*, Fe ore tailings were throughly amended with 2% (w/w) Lucerne hay (ground to below 1 mm, 43.2% C and 4.1% N, with a C/N ratio of 10.6) (Petbarn Ltd., Australia), and

inoculated with a native soil microbial inoculum (rich in *Actinobacteria* (62.3%), *Chloroflexi* (11.46%) and *Proteobacteria* (8.45%) at phylum level) in soil suspension (soil: water was 1:12 w/v). The mixture was incubated for 1 month with a moisture of 55% water holding capacity. The tailing at this stage was called "early technosol" in the present study.

In "***advanced technosol" formation process***, a pot experiment under glasshouse conditions was conducted. Three pioneer plant species were cultivated in river sand for 1 month and then transplanted in the "early technosol", including (1) *Atriplex amnicola*, (2) *Maireana brevifolia* and (3) Silk Sorghum grass (*Sorghum* spp. Hybrid cv. Silk). Besides, a control treatment without plants were also included. The seeds of *Atriplex amnicola* and *Maireana brevifolia* were purchased from Nindethana Ltd., Australia. The seeds of *Sorghum* spp. Hybrid cv. Silk were purchased from Pukalus's farm in Injune origin, Queensland, Australia. Half of the "early technosol" were amended with 10% (w/w) native soil (see its detailed characteristics at Table S1) to assist plant colonization and stimulate pedogenesis. Native soils were sterilized twice by autoclave at 121°C for 40 min to eliminate the soil microbial effects. Based on previous studies, the soil were mainly composed of quartz, Fe-kaolinite, ferrihydrite-Si, and goethite etc.[10] The reasons for using native soil are: 1) to improve physical and chemical properties in tailings through direct addition of key secondary minerals (the soil is rich in kaolinite, hematite, and with well aggregate structure) to support the plant root development, and speed up pedogenesis in the tailings; 2) the soils were the mostly easily acquired materials in the mine site, and are ideal materials for direct improvement of physical and chemical characteristics of the tailings. There were 8 treatments, with 4 replicates for each treatment, totalling 32 pots. Each pot had 1.5 kg of "early technosol". Seeds were germinated in petri dishes until 2-cm length seedlings developed, which were then transplanted into river sand (amendment of nutrient solution (Flowfeed EX7, Grow Force, Australia) for pre-culturing. The seedlings were cultivated in river sand for 1 month before transplantation to the "early technosol". The plants were cultivated in "early technosol" for additional 3.5 months before harvest. The pots were daily watered and maintained at 55% of water holding capacity of the tailings technosol. The plants were cultivated in a controlled glasshouse with 25°C, 14/10 h (light/dark), and the light intensity of 600-1200 μmol m^{-2} s^{-1}. Porewater were collected at 1, 2 and 3.5 months after transplantation by using rhizo samplers (pore volume size 0.15 μm, Rhizosphere Research Products, Netherlands), which were inserted and kept in the tailings all through the plant cultivation processes.

At harvest, the plant roots and shoots were separately sampled, washed carefully with MilliQ water and oven-dried at 70°C for 96 h. The dry weight of the plant shoots and roots were weighed and plant elemental concentration were detected by ICP-OES (720ES, Varian Inc., Palo Alto, California, USA) after digestion by concentrate HNO_3.[58] A certified standard reference material (NIST-SRM 1515 Apple Leaves) was used for quality control. About 20 g of the fresh tailing samples were freeze-dried at -55°C for 48 h, and thoroughly ground for bulk XRD and synchrotron-based Fe K edge XAFS analysis. The remainders of tailing samples were air-dried for physical and chemical analysis. Tailings in this stage were called "advanced technosol".

Geochemical characterization

The initial tailings, "early technosol" and "advanced technosol", and native soils were air-dried for geochemical analysis. The pH and electrical conductivity (EC) were determined via solid: water ratio of 1:5 (w/w) by a pH electrode (TPS 900-P) and an EC electrode (TPS 2100). Total organic carbon (TOC) was determined using a LECO CNS-2000 Analyser (LECO Corporation, MI, USA) after removing inorganic carbon by 5 mol L^{-1} HCl.[59] Total nitrogen (TN) was determined by a LECO CNS-2000 Analyser. Acid ammonium oxalate (AAO) extractible and citrate/bicarbonate/dithionite (CBD) extractible Fe, Al, K, Mg, Ca and P in the tailings were analysed according to Rayment and Lyons (2011).[60] Briefly, 0.5 g tailings were extracted in 40 mL AAO solution (0.175 M $(NH_4)_2C_2O_4$ + 0.1 M $H_2C_2O_4$) or 40 mL CBD solution (0.3 M Na3C6H5O7 + 0.125 M $NaHCO_3$ +1 g Na2S2O4). After shaking for 16 h in the dark, the mixture suspensions were filtered through 0.45 μm membrane. Elemental concentrations in the filtrates were analysed by using an ICP-OES (720ES, Varian Inc., Palo Alto, California, USA).

For the porewater chemistry, the pH and EC in porewater samples were analyzed by pH electrode (TPS 900) and an EC electrode (TPS 2100). TOC and TN were analyzed by using TOC analyzer with TN detector (VCPH, Shimazu, Japan). Elements such as Fe, Si, Al, K, Ca, Mg were determined by ICP-OES. Quality controls were processed by repeatedly detection of standard solutions of relevant elements. The organic acids in the porewater samples were detected by Ion Chromatography with conductivity detector (ICS-2100, Dionex, Sunnyvale, CA, USA).

DNA isolation and microbial community analysis

DNA was extracted from tailings of different treatments by using the DNeasy PowerSoil Kit (Qiagen). The DNA quality was checked by using NanoDrop®ND-2000 (Thermo Scientific, USA). High quality DNA was sent to the Australian Centre for Ecogenomics, the University of Queensland, for paired-end amplicon sequencing on an Illumina MiSeq platform.[61] The V6-V8 regions of the 16S rRNA gene were amplified by using the primer set 926F (5′-AAACTYAAAKGAATTGACGG-3′) and 1392wR (5′-ACGGGCGGTG WGTRC-3′), for prokaryotic microbial communities analysis.[62] All raw sequencing data in this study are stored in NCBI Sequence Read Archive under BioProject accession No. PRJNA727935 (note: DNA sequencing data from treatments "TL" and "TL-Mb" are in No. PRJNA714455).

Raw sequencing reads ("fastq" file) were examined by using FastQC v0.11.4 (http://www.bioinformatics.babraham.ac.uk/projects/fastqc). Paired read files and the associated metadata were imported into a "qza" artifact, according to the QIIME2 (Quantitative Insights Into Microbial Ecology 2, version 2019.1) protocol.[63] Adaptor and primers were trimmed using cutadapt.[64] The paired read were joined using vsearch and low quality reads were removed from the dataset using default settings ($Q < 20$). Sequences were clustered to operational taxonomic units (OTUs) (with 97% similarity) after removing low quality, replicated reads and chimeras by using deblur.[65] Sequences with low relative abundance (below 0.1%) were removed from the resulting feature tables. Taxonomy assignment was uclust against greengenes database for the 16S rRNA sequences. The resultant quality-filtered OTUs tables were rarefied and imported into R (v3.4.1). Diversity assessment of microbial community was performed on the rarefied dataset. The Shannon indices were calculated based on OTU information by using "vegan" package (2.4.4).[66] Principal component analysis (PCA) of prokaryotic microbial communities in early technosol and advanced technosol with different treatments were conducted by CANOCO 5.0 (Microcomputer Power, Ithaca, NY, USA). Similarity (ANOSIM)[67] were analysed by using "vegan" package (2.4.4). The microbial abundances data used for PCA were logarithmically transformed and checked for normality through quantile–quantile (Q–Q) plot and Kolmogorov–Smirnov (K–S) test using the statistical package SPSS (Ver 18, IBM, Armonk, NY, USA).

Water stable aggregate assessment

The water stable aggregate was analysed by the wet-sieving method modified from Kemper and Rosenau (1986).[68] Briefly, 50 g air-dried EE tailings/soil samples were put on the series of sieves (2000 μm, 250 μm, 53 μm) and submerged into distilled water for 3 min. Then the fractions of different sizes were separated through FRITSCH Analysette 3-laboratory model of vibration sifting device (Fritsch, Germany). The parameters for the vibration were three 20-sec shakes at an amplitude of 0.5 mm for a total shaking time of 1 min. Through this way, three water-stable aggregate fractions: including (1) 2000-250 μm (fraction containing macroaggregates); (2) 250-53 μm (fraction containing microaggregates); and (3) < 53 μm (discrete particles) were collected and air-dried. The percentage of water stable aggregates (WSA) of different sizes was expressed as the ratio of WSA fraction to the total dry weight of the samples. The mean weight diameter (MWD) of WSAs were calculated as follows:

$$MWD = \sum_{k=1}^{n+1} \frac{r_k + r_{k-1}}{2} \times m_k$$

where k = 1, 2, 3, representing different fractions, r_0=2000 μm, r_1=250 μm, r_2=53 μm, m_k is the proportion of aggregate fractions on the k^{th} sieve, and n is the number of the sieves.

The isolated microaggregates (53-250 μm) and macroaggregates (250-2000 μm) from the early technosol and advanced technosol and soils were air-dried (mimic the natural conditions) for XRD, XPS, ATR-FTIR, synchrotron-based Fe K edge XAFS, as well as synchrotron based XFM, BSE-SEM-EDS and NanoSIMS analysis. The air-dried microaggregates were further used for colloidal fraction isolation. Besides, some intact microaggregates were embedded by epoxy resin and oven-cured at 60°C, polished and carbon coated for BSE-SEM-EDS and Mineral Liberation Analysis (MLA) analysis.

Isolation of colloids from microaggregates of early technosol, advanced technosol and native soils

The colloid fraction in the tailing technosols and soils are usually the most active part.[42] The colloidal fraction was extracted from air-dried microaggregates by using the procedure of Schumacher et al. (2005).[69] Briefly, air-dried tailing/soil aggregates were suspended in deionized water at the ratio of 1:5 (W/V) (10g into 50 mL tubes), shaken for 8 h at 25°C, and centrifuged for 6 min at 2,500 g. Both the deposits

(non-colloidal fraction) and the supernatant suspensions (colloidal fraction) were freeze-dried and ground for XRD, Fe K edge XAFS analysis and C 1s NEXAFS, as well as ATR-FTIR analysis. There were no colloids in the initial tailings and early technosol, therefore we only detected the colloids from advanced technosol and native soil in the study.

Micro-spectroscopic analysis

XRD and ATR-FTIR analysis

The freeze-dried and ground (fine powder, size < 7 μm) samples (including whole bulk tailings, colloids and sediments in microaggregates) were subject to XRD analysis using a Bruker D8 DISCOVER diffractometer, with the Bragg-Brentano θ–2θ reflecting geometry equipped with a Johansson-type focusing Ge primary monochromator and a linear silicon strip detector LynxEye (open to 2.896°). XRD spectra data were collected between 4° and 70° with a step of 0.02°, and the spectra were processed using the Diffrac^{plus} Evaluation Package V4.2 (Bruker AXS, Germany) and the PDF-4 mineral database (2019 release). Functional groups of minerals and/or organic groups in the tailing colloids of different treatments were determined by attenuated total reflection Fourier-transform infrared (ATR-FTIR) using a Cary 630 FTIR with Diamond ATR module (Agilent Technologies, Palo Alto, CA, USA). Spectra were collected between 400 and 4000 cm^{-1} with a resolution of 2 cm^{-1}, totalling 64 scans. ATR-FTIR spectra were processed by MicroLab software package and Origin 8.5 (OriginLab Corporation, Northampton, MA, USA). The average absorbance value in the range from 2095 cm^{-1} to 2105 cm^{-1} were used as the internal standard for the normalisation of ATR-FTIR spectra, which were chosen based on the stability and continuity of the spectra.

Fe K edge XAFS analysis

Fe K-edge (7,112 eV) XAFS spectra of the freeze-dried and ground (fine powder, size < 7 μm) samples (including whole bulk, colloids, and non-colloids in microaggregates) from tailings, technosols and native soils were collected on beamline 01C1 and 17C1 at the national synchrotron radiation research centre (NSRRC) in Taiwan, as well as XAS beamline of Australia synchrotron. Various Fe standards were used, including magnetite, hematite, goethite, ferrihydrite, siderite, Fe(III) phosphate, jarosite, biotite, olivine, illite, epidote, vermiculite, pyrite, Fe(II) gluconate hydrate, Fe(II) glutathione, and Fe(III) citrate. Besides, Fe(III)-Si-short range ordered minerals (hereafter named Fe(III)-Si-SRO) and ferrihydrite-silica (silica binding to 2L-ferrihydrite, hereafter termed Fh-Si) were also included to represent Fe-Si rich secondary minerals with poor polymerization. Hematite, goethite, magnetite, siderite, pyrite, Fe(III) phosphate, Fe(III)-citrate, and Fe(II) gluconate hydrate jarosite were purchased from Sigma Aldrich. Olivine, biotite, epidote, vermiculite and illite were obtained from Ward's science (https://www.wardsci.com). Ferrihydrite (2-line) was synthesised according to Schwertmann and Cornell (2000).[43] Briefly, 40 g $Fe(NO_3)_3 \cdot 9H_2O$ was dissolved in 500 mL MilliQ water and 1.0 M KOH was added to adjust the pH to 7-8. The products were centrifuged, dialysed and freeze-dried before use. Fe(III)-organic matter complexes were prepared by mixing 0.1 M Fe(III) solutions with oxalate acid at a ratio of 1:5 mole. The Fe(III)-Si-SRO were synthesized by hydrolysing Fe(III) nitrate in the presence of SiO_3 ligands (Na_2SiO_3) at ca. pH=9 at a resulting Si to Fe proportion of 1 (modified from Pokrovski et al (2003).[70] Fh-Si was synthesized by adding 2 g 2L-ferrihydrite into 20 mL silicic acid solutions (10 mmol L^{-1}) under the pH 7, and the reaction lasted for 3 days with gentle shaking. The Fe(III)-Si-SRO and Fh-Si minerals were collected through centrifugation at 3,000 ×g for 5 min followed by freeze-drying.

The collected XAFS spectra range was from -200 to 800 eV (relative to the Fe K edge absorption) with the following processes: -200 to -20 eV (10 eV steps with 2 sec per step); -20 - 30 eV (0.35 eV steps with 2 sec per step); 30 - 800 eV (4 eV steps with 4 sec per step). The XAFS spectra were collected at transmission mode, the energy was calibrated by using a Fe foil as an internal standard (calibration energy is 7112.0 eV). The XAFS spectra were baseline and background corrected and normalised by using ATHENA from DEMETER (or IFEFFIT) software package (CARS, University of Chicago).[71] The X-ray absorption fine structure spectroscopy were processed by principal component analysis (PCA), based on which magnetite, goethite, ferrihydrite, siderite, biotite, ferrous oxide, hematite, Fe(III)-Si-SRO, Fh-Si, were selected for linear combination fitting (LCF) analysis of the the extended X-ray absorption spectra (EXAFS, *k* space from 2.5 to 11.5) (Figure S25) by using the ATHENA software package.[71] The quality control of the fitting were confirmed by minimal R-factor, Chi-square and Reduced Chi-square.

C 1s NEXAFS analysis

The freeze-dried and ground (fine powder, size < 7 μm) samples (including whole bulk, colloids, and non-colloids in microaggregates) from tailings, technosols and native soils were subject to C1s NEXAFS analysis for organic C forms analysis in the beamline 20A1 of NSRRC, Taiwan. Each spectrum was acquired in the total electron yield (TEY) mode, from 272 to 317 eV, with energy resolution of 0.01 eV and X-ray spot size of 2 mm^2, using beamline 20A1, NSRRC, Taiwan. The spectra was averaged (3-4 scans for each sample), calibrated, base-line corrected and edge-step normalised by using ATHENA software from DEMETER (or IFEFFIT) software package (CARS, University of Chicago) (Ravel et al., 2002). Organic C standards including graphite (solely aromatic C), L-glucose (solely O-alkyl C), Na formate (solely carboxyl C), L-glutamic acid (alkyl C, carboxyl C), citric acid (alkyl C and carboxyl C) and N,N'-Methylenebis (acrylamide) (rich in carbonyl C) were used for verifying the organic C forms, which were purchased from Sigma Aldrich (Castle Hill, NSW, Australia). Their C 1s NEXAFS spectra are shown in Figure S26. After basal line correction and edge step normalization, the C 1s NEXAFS spectra were deconvoluted in energy range 280-294 eV according to (Solomon et al. 2005), using the "peakfit" package of ATHENA software from DEMETER (or IFEFFIT) software package (version 0.9.26). A arctan function (energy 291.0 eV; height 1; FWHM 0.5 eV) representing the edge step was fitted. Then Gaussian peaks at around 285.2eV, 286.4eV, 287.4eV, 288.4eV, 289.4eV, 290.4eV representing aromatic C, phenolic C, alkyl C, carboxyl C, O-alkyl C and carbonyl C respectively (Figure S27) were fitted. Besides, a Gaussian peak at around 292eV (represents broad 1s ➔ σ* transitions of saturated single covalent bonds (Solomon et al. 2005)[72]) was also included in the fitting to enhance the fitting quality. The heights of the Gaussian peaks were initially set to 1eV and their width were set to 0.4 eV, but allowed to float during the fitting. The percentage of different organic forms were calculated as quotient of the area of their respective Gaussian peaks divided by the sum of the areas of peaks (except the peak at 292eV) (Prietzel et al. 2018).[73]

XFM analysis

Synchrotron-based XFM analyses were conducted at the XFM beamline at the Australian Synchrotron (Melbourne, Australia). Air-dried intact aggregate samples were selected under microscopy and embedded by epoxy resins (Araldite kit 502, electron microscope sciences, Hatfield) and polished with a clean fixed diamond to gain a 30-μm thick petrographic thin section. According to Steffens et al. (2017),[74] chemical embedding is a suitable for obtaining intact microscale structures with no distortion during drying and polishing. The petrographic aggregate thin sections were then mounted on quartz slides and attached to a Perspex sample holder using Mylar tape and then placed on the translation stages of the X-ray microprobe. A Si (111) monochromatic X-ray beam was scanned onto the samples via the Kirkpatrick-Baez mirrors, with the spot size of 2 μm x 2 μm.[75] The X-ray fluorescence emitted by the samples was collected by using the 384-element Maia detector.[76] An initial survey scan was conducted to get an overview of the key elemental distribution to help select the area of interest, with a sampling interval of 12 μm and a dwell time of 0.67 msec per pixel. Then interested area were further analysed by high-resolution mode via an interval of 2 μm with the dwell time 0.4 msec (stage velocity of 5 mm/sec). The raw data of elemental distribution were analysed using GeoPIXE and the images were generated using the Dynamic Analysis method.[77]

MLA analysis

The same thin sections of technosol and soil aggregates used for XFM analysis was coated by carbon for Mineral Liberation Analysis (MLA) analysis by using automated scanning electron microscope based MLA located in JKMRC, SMI, the University of Queensland, Australia.[30] The samples were analyzed with a grain X-ray mapping measurement mode (GXMAP) coupled with back scattered electron (BSE) spectroscopy with electron beam accelerating voltage of 25 kV. The details can be seen in Fandrich et al. (2007).[78]

BSE-SEM-EDS analysis

The same thin sections of technosol and soil aggregates used for XFM and MLA analysis was coated by carbon for BSE-SEM-EDS analysis at Hitachi SU3500 SEM (at an accelerating voltage of 5-20 kV) equipped for electron dispersive X-ray spectroscopy (EDS, with Oxford). For surface mineral morphology analysis, the entire air-dried water stable aggregates from EE tailings/soils were coated by carbon, and analysed by Hitachi SU3500 SEM. Back scattered electron (BSE) imaging was conducted under an accelerating voltage of 20 kV (spot size 50 nm), and an electron dispersive X-ray spectroscopy (EDS) were used to detect elemental composition in selected areas. For samples from each treatment, 5-8 aggregates were randomly selected and examined under BSE-SEM-EDS and MLA analysis.

TEM-SAED analysis

The colloidal fractions isolated from microaggregates of advanced technosol were deposited on the copper grid (200 mesh, ProSciTech Pty. Ltd., Queensland, Australia), and air-dried in the desiccator. The samples were analysed by using the aberration-corrected Hitachi HF5000 S/TEM at 200 keV, in Centre for Microscopy and Microanalysis, The University of Queensland, Australia. The machine was equipped with an energy dispersive X-ray spectroscopy (EDS, Oxford EDX 2x1sr 100mm SDD EDX) detectors. TEM images were recorded by a CCD camera. Electron diffraction patterns were acquired in selected area and recorded.

NanoSIMS analysis

The free, air-dried water stable aggregates were gently dispersed into the pure water (1:10), and shaken according to Kopittke et al. (2017).[79] Following this way, the organo-mineral associations are assumed to be maintained for NanoSIMS analysis. *In situ* isotopic mapping was done using NanoSIMS 50L (Cameca, Gennevilliers, France) located at the Centre for Microscopy, Characterisation and Analysis at University of Western Australia. Analyses using a 16 keV Cs^+ primary ion beam were conducted in multi-collection mode simultaneously detecting negative secondary ions ^{12}C, $^{14}N^{12}C$, ^{28}Si, $^{27}Al^{16}O$ and $^{56}Fe^{16}O$. The mass spectrometer was tuned to high mass resolution of 10,000 (CAMECA definition), sufficient to separate all ion species of interest from any interferences, using an entrance slit of 30 μm and aperture slit of 200 μm. Pure metal standards–Astimex standard ref (Astimex standards Ltd, Ontario, Canada) were used to identify ion species of interest. For secondary ion imaging, the primary current was set to 2 pA using a 350-μm primary aperture, giving a spot size of 100 nm. Twenty individual aggregates (or groups thereof) were randomly selected and analysed using a 20 x 20 μm analyses (256 pixel resolution). All analysis areas were implanted to the same ion dose (6 $x10^{16}$ ions per cm^2) prior to each acquisition. Images were processed using the OpenMIMS data analysis software (National Resource for Imaging Mass Spectrometry http://nrims.harvard.edu) for the freeware package ImageJ (National Institutes of Health, Bethesda, MD, USA). Images were corrected for detector dead time (44 nsec) on individual pixels.

C 1s XPS analysis

The ground tailing/soil aggregate samples were processed for the XPS analyses using a Kratos AXIS Ultra with a monochromatic Al X-ray source at 225 W under ultrahigh vacuum conditions. A survey scan from 0 to 1200 eV were firstly conducted (dwell time: 100 ms), then the high resolution C1s (sub-peak centered at 285 eV) analysis was conducted. The detailed set for C 1s XPS: the pass energy, 20 eV; step, 50 meV; the dwell time, 250 ms. XPS data was processed by CasaXPS software package.

QUANTIFICATION AND STATISTICAL ANALYSIS

The significant differences in porewater chemical traits, physicochemical characteristics and water stable aggregate percentage among different treatments were assessed by one way ANOVA followed with Tukey's test ($P < 0.05$) by using SPSS software package (Ver 18, IBM, Armonk, NY, USA). The physicochemical data were checked for normality through quantile–quantile (Q–Q) plot and Kolmogorov–Smirnov (K–S) test using SPSS software package (Ver 18, IBM, Armonk, NY, USA) and subject to principal component analysis (PCA) using CANOCO 5.0 (Microcomputer Power, Ithaca, NY, USA).